AERODYNAMIC CHARACTERISTICS OF A WEDGE AND CONE AT HYPERSONIC MACH NUMBERS

Thesis by

Lt. Richard D. DeLauer, USN

In Partial Fulfillment of the Requirements

For the Degree of

Aeronautical Engineer

California Institute of Technology

Pasadena, California

1950

ACKNOWLEDGMENTS

The author wishes to express his appreciation to Dr. H. Nagamatsu for his valuable discussion and advice for carrying out this investigation. He also wishes to express his appreciation to Miss S. Woodbury for her suggestions and typing in the preperation of this thesis, and to Mrs. Katherine McColgan, Aeronautics Librarian, for her assistance in the early phases of the investigation.

The author was assisted in carrying out this investigation by Lt. Lee R. Scherer, USN.

ABSTRACT

The problem of predicting the aerodynamic characteristics of configurations at hypersonic Mach numbers has been unreliable due to the lack of experimental data.

By predicting the aerodynamic characteristics of a wedge and cone at Mach numbers from 2 to 12 by four different supersonic theories, a basis for future experimental comparison was provided.

An attempt was made to correlate the theoretical result of a 20^{o} wedge and cone with wind tunnel test results of the same configuration. However, due to scheduling difficulties the experimental phase was not completed in time enough to be included in this report.

The theoretical results indicate that the hypersonic similarity solution gives close agreement with the exact solution for large Mach numbers. The linearized and second order theory deviates from the exact solution for Mach numbers greater than 3.

TABLE OF CONTENTS

LIST OF FIGURES

LIST OF FIGURES (continued)

LIST OF TABLES

LIST OF TABLES (continued)

SYMBOLS AND NOTATION

The following are the symbols and notation with their definitions used in this investigation.

p_i — static pressure of the flow. The subscripts denote flow field (i.e.)

- 1 - free stream
- 2 - flow behind shock or on body
- o - stagnation conditions
- s - flow on surface of body.

C_p — pressure coefficient = $\Delta p/q$.

q — free stream dynamic pressure = $\frac{1}{2}\rho_1 U_1^2 = \frac{\gamma}{2} p_1 M_1^2$

U_1 — free stream velocity.

a_i — speed of sound $a_i = \sqrt{\gamma p_i/\rho_i}$. Subscript indicates some conditions as pressure p_i.

ρ_i — fluid density. Subscripts same as for p_i.

M_i — Mach number = u_i/a_i. Subscripts same as p_i.

β — inclination of shock wave, or the quanity $\sqrt{M_1^2 - 1}$

γ — ratio of specific heats = 1.4 for air.

r, θ — cylindrical or spherical coordinates.

x_i — Cartesian coordinates. Subscripts denote orthogonal directions of axis.

u, v — velocity components.

SYMBOLS AND NOTATION (continued)

u_i, v_k	indicate $\frac{\partial u}{\partial i}$, $\frac{\partial v}{\partial k}$ where i, k are coordinates of system being used.
θ	semi-apex angle of cone or wedge, and flow deflection in one case.
ϕ	potential notation.
α	angle of attack.
ξ, η, t	non-dimensional coordinates, or variables of integration.
δ	body thickness, or total apex angle.
b	body length.
k	thickness ratio parameter ($M_1 \delta/b$).

I. INTRODUCTION

The purpose of this investigation was to determine the aerodynamic characteristics of a wedge and cone at hypersonic Mach numbers and to correlate these results with existing theories.

Since there has been little or no experimental data available at extremely high Mach numbers, the reliability of extending existing supersonic theory to hypersonic flow is questionable. The problem is vast, including as it does, the question of viscosity, shock waves and deviations from a perfect gas. However, in this investigation only one phase was to be considered that of correlating, without corrections for viscosity, shock waves and deviations from a perfect gas, the experimental results of one configuration of a wedge and a cone with the various supersonic theories. Also an attempt was made to predict, theoretically, the surface pressure on various configurations of wedges and cones by four different theories covering the range of speeds from Mach number 2 through 12, thus providing a basis of comparison for future experimental work.

The configurations used in the theoretical investigation were:

1. Wedge with apex angles of 5°, 10°, 20°, 30°, 40°, 50° and 60° at angles of attack of 0°, 2°, 4°.
2. Cone with apex angles of 5°, 10°, 20°, 30°, 40°, 50° and 60° at zero angle of attack.

In the experimental phase the only configurations to be tested were the

wedge and cone with a 20° apex angle.

The four methods used in determining the theoretical pressure distributions were:

1. Oblique Shock-Wedge; Exact Theory for Cone
2. First Order Theory - Linearized Theory
3. Second Order Theory - Iteration of Linearized Theory
4. Hypersonic Similarity.

A brief discussion of each of the above theories is given on pages 3 to 19.

Due to scheduling difficulties in the hypersonic tunnel, the experimental phase of this investigation was not concluded in time to have the results included in this report, However, as the experimental portion of the investigation is to be continued, the correlation of test results with the theoretical results presented in this report will be made at a later date.

Figs. 1, 2, 3 and 4 give sketches and photographs of the models that will be used in the experimental phase.

II. CALCULATIONS BY THE VARIOUS THEORIES

A. Oblique Shock Theory - Wedge

From the normal shock theory, the relation for the pressure rise across the shock to the free stream pressure is given as (cf. Ref. 1)

$$p_2 - p_1 / p_1 = \frac{2\gamma}{\gamma+1} [M_1^2 - 1] \tag{1}$$

To transform this equation for use in case of oblique shock waves it is only necessary to replace M_1 by $M_1 \sin \beta$, where β is an inclination of the shock wave.

$$p_2 - p_1 / p_1 = \frac{2\gamma}{\gamma+1} [M_1^2 \sin^2 \beta - 1] \tag{2}$$

The pressure coefficient C_p is defined as

$$C_p = p_2 - p_1 / q \tag{3}$$

where q is the free stream dynamic pressure, and is equal to

$$q = \frac{1}{2} \rho_1 U_1 = \frac{\gamma p_1}{2} \frac{\rho_1 U_1}{\gamma p_1} = \frac{\gamma}{2} p_1 M_1^2 \tag{4}$$

since $M_1 = U_1 / a_1$ and $a_1 = \sqrt{\gamma p_1 / \rho_1}$

and by substituting Eqs. (2) and (4) into Eq. (3), the pressure

coefficient becomes

$$C_p = \frac{p_2 - p_1}{\gamma p_1 M_1^2/2} = \frac{4}{M_1^2(\gamma+1)} \left[M_1^2 \sin^2\beta - 1\right] \tag{5}$$

with $$\frac{1}{M_1^2} = \sin^2\beta - \frac{\gamma+1}{2} \frac{\sin\beta \sin\theta}{\cos(\beta-\theta)}$$

The resulting pressure coefficients based on Eq. (5) are given in Tables 1 to 3 and plotted on Figs. 5 to 7.

B. Exact Solution for Cone

The equation for steady isentropic flow in spherical coordinates with axial symmetry is given as (cf. Ref. 2)

$$(a^2 - u^2) u_r + \frac{(a^2 - v^2)}{r} v_\theta - uv\left(\frac{1}{r} u_\theta + v_r\right) + a^2 \frac{2u + v\cot\theta}{r} = 0 \tag{6}$$

where direction of velocity and coordinates are

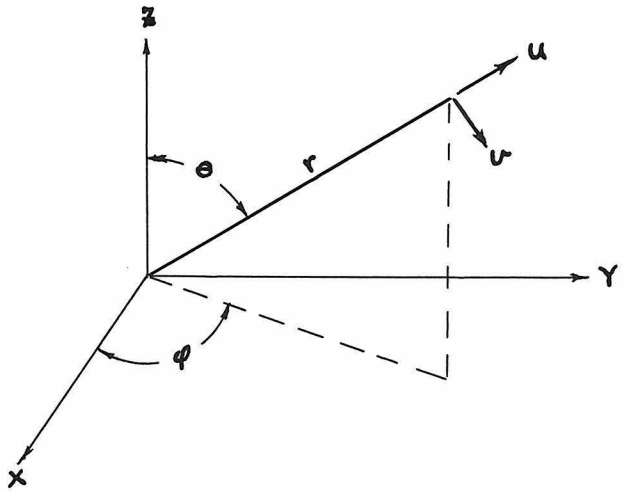

For the case of flow past the unyawed cone, it is assumed that all fluid properties are constant on any conical surface having the same vertex and axis of symmetry as cone itself.

If the coordinate axis are placed at the vertex of the cone, the above assumption results in the fluid properties being independent of r. The irrotationality equation for this case is

$$v_r + \frac{v}{r} - \frac{1}{r} u_\theta = 0 \tag{7}$$

From the basic assumption that the flow is independent of r, the irrotationality equation becomes

$$\frac{du}{d\theta} = v \tag{8}$$

and Eq. (6) becomes

$$\frac{dv}{d\theta} + u + \frac{a^2}{a^2 - v^2}(u + v \cot\theta) = 0 \tag{9}$$

By integrating this equation it is possible to evaluate the flow field. Kopal has done this integration by a numerical method and has tabulated the results (cf. Ref. 3). Kopal has also tabulated the ratio of pressure on the cone to that immediately behind the shock wave, and the ratio of the pressure immediately behind the shock wave to that of the undisturbed free stream, i.e., p_s/p_2 and p_2/p_1 respectively. The

product of these ratios gives p_s/p_1, which in turn makes it possible to calculate the pressure coefficient

$$C_p = \frac{2}{\gamma M_1^2} (p_s - p_1)/p_1 \qquad (10)$$

The results of this calculation are tabulated in Table 4 and are plotted on Fig. 8.

C. First Order Theory - Wedge

By linearizing the equations of motion and assuming that the flow is irrotational, a perturbation potential may be introduced (cf. Ref. 4). The linearized equation of motion becomes

$$\left(1 - \frac{U^2}{a_1^2}\right) \frac{\partial u_1'}{\partial x_1} + \frac{\partial u_2'}{\partial x_2} + \frac{\partial u_3'}{\partial x_3} = 0 \qquad (11)$$

where

$u_1 = U = \text{const.}$	$u_1 = U + u_1'$
$u_2 = 0$	$u_2 = u_2'$
$u_3 = 0$	$u_3 = u_3'$
(away from body)	(neighborhood of body)

Introducing the perturbation potential

$$u_i' = \frac{\partial \phi'}{\partial x_i} \qquad (12)$$

the equation of motion becomes

$$\left(1 - \frac{U^2}{a_1^2}\right) \frac{\partial^2 \phi'}{\partial x_1^2} + \frac{\partial^2 \phi'}{\partial x_2^2} + \frac{\partial^2 \phi'}{\partial x_3^2} = 0 \qquad (13)$$

For consistancy the same approximation for determining the pressure coefficient was made. From the isentropic relationship, the pressure ratio is

$$p_2 / p_1 = \left[\frac{1 + \frac{\gamma-1}{2} M_1^2}{1 + \frac{\gamma-1}{2} M_2^2} \right]^{\gamma/\gamma-1} \qquad (14)$$

which reduces to

$$p_2 / p_1 = \left[\frac{1}{1 + \frac{\gamma-1}{2} M_1^2 \; 2 \, u'/U} \right]^{\gamma/\gamma-1} \qquad (15)$$

and

$$p_2 / p_1 = 1 - \frac{\gamma}{2} M_1^2 \; 2 \, u'/U + \cdots \qquad (16)$$

and since

$$\frac{\gamma}{2} M_1^2 p_1 = \frac{1}{2} \rho_1 U_1^2$$

$$C_p = -2 \, u'/U \qquad (17)$$

By finding a solution which satisfies both the boundary conditions as well as the perturbation equation, the pressure coefficient equation becomes

$$C_p = \frac{2}{\sqrt{M_1^2 - 1}} \left[\frac{dx_2}{dx_1} \right]_{\text{boundary}} \tag{18}$$

or for the case of the wedge

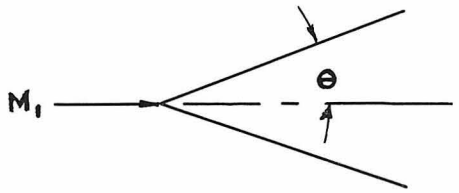

$$C_p = \frac{2}{\sqrt{M_1^2 - 1}} \text{ TAN } \theta \tag{19}$$

Table 5 gives the values of C_p for a wedge at zero angle of attack as calculated by the first order theory, and a plot of C_p vs Mach number is given on Fig. 9.

In calculating the pressure coefficients for the wedge at angles of attack (2°, 4°) by the linearized theory the same equation as used for the zero angle of attack calculations will hold.

$$C_p = \frac{2}{\sqrt{M_1^2 - 1}} \left[\frac{dx_2}{dx_1} \right]_{\text{boundary}} \tag{18}$$

However, for this case the slope of the upper and lower surfaces will differ by the angle of attack. For the case of positive angle of attack

$$C_{p\ upper} = \frac{2}{\sqrt{M_1^2 - 1}} \tan(\theta - \alpha) \qquad (20)$$

$$C_{p\ lower} = \frac{2}{\sqrt{M_1^2 - 1}} \tan(\theta + \alpha) \qquad (21)$$

where

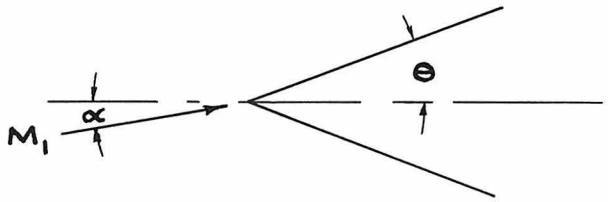

Tables 6 and 7 give the calculated first order value of the wedge at angles of attack of 2°, 4°, and their plot versus Mach number is given on Figs. 10 and 11.

D. First Order Theory - Cone

The linearized potential equation in cylindrical coordinates assuming axial symmetry is

$$\frac{\partial^2 \phi}{\partial r^2} + \frac{1}{r}\frac{\partial \phi}{\partial r} + \left(1 - \frac{U^2}{a^2}\right)\frac{\partial^2 \phi}{\partial x^2} = 0 \qquad (22)$$

By assuming that the effects of infinitesimals can be superimposed, the potential of the additional velocities has the form

$$\phi(x,r) = \int_0^{x-\beta r} f(\xi)\ \frac{d\xi}{\sqrt{(x-\xi)^2-\beta^2 r^2}} \tag{23}$$

where $\beta = \sqrt{\frac{U}{a^2} - 1}$

By assuming the vertex of the body at $x = 0$, this integral can be transformed by letting $\frac{x-\xi}{\beta r} = \cosh u$. Then the potential becomes

$$\phi = \int_{\cosh^{-1}\frac{x}{\beta r}}^{0} f(x - \beta r \cosh u)\, du \tag{24}$$

and the velocities components are

$$\frac{\partial \phi}{\partial x} \quad \text{and} \quad \frac{\partial \phi}{\partial r} \tag{25}$$

Von Kármán solved the above equation in (Ref. 5) and the solution for the over-pressure acting on the surface of the cone is

$$\Delta p = \rho U^2 \theta^2 \frac{\cosh^{-1}\frac{1}{\theta\beta}}{\sqrt{1 - \frac{\theta^2}{\beta^2} + \theta \cosh^{-1}\frac{1}{\theta\beta}}} \tag{26}$$

or approximately

$$\Delta p = \rho U \theta \, \mathrm{Log}_e \left(\frac{2}{\theta \beta} \right) \tag{27}$$

from which

$$C_p = 2 \theta^2 \, \mathrm{Log}_e \frac{2}{\theta \sqrt{M_1^2 - 1}} \tag{28}$$

where θ = semi-apex angle.

The calculated values of the pressure coefficient, C_p, for the first order solution of the cone is given in Table 8 and the plot of C_p vs Mach number is given on Fig. 12.

E. Second Order Theory - Wedge

The linearization method which led to the Prandtl-Glauert equation can be considered to be the first step in an iteration procedure corresponding to the general technique of solution by successive approximation based on the theory of perturbations.

Busemann (Ref. 6), has carried out the iteration process for supersonic flow in which the potential function is expanded in a power series in a parameter proportional to the thickness ratio of the body. Busemann's result to the second order for plane flow for the pressure coefficient is

$$C_p = \pm \frac{2}{\sqrt{M_1^2-1}}\,\theta + \left[\frac{\gamma M_1^2 + (M_1^2-2)^2}{2\,(M_1^2-1)^2}\right]\theta^2 \qquad (29)$$

This equation was used to compute the C_p for the wedges under consideration. In this equation θ is the angle of flow deflection, for zero angle of attack it corresponds to the wedge semi-apex angle.

Tables 9, 10 and 11 give the calculated second order values of C_p for the wedge. The plot of these values are given on Figs. 13, 14 and 15.

F. Second Order Theory - Cone

For axially-symmetric flow the problem of determining a second order approximation is reduced to first order problem by the discovery of a particular solution of the iteration equation. The iteration equation for a cone as given by Van Dyke, (Ref. 7), is

$$(1-t^2)\,\bar{\varphi}_{tt} + \frac{\bar{\varphi}_t}{t} = M_1^2\left[2(N-1)t^2\,\bar{\Phi}_{tt}(\bar{\Phi} - t\bar{\Phi}_t) - 2t\,\bar{\Phi}_{tt} + \bar{\Phi}_t + \beta^2\bar{\Phi}_{tt}\bar{\Phi}_t^2\right] \qquad (30)$$

where the concial non-orthogonal coordinates are (x, t) and

$$t = \beta r/x \qquad \beta = \sqrt{M_1^2 - 1} \qquad N = \frac{(\gamma+1)M_1^2}{2\beta^2}$$

$$\Phi(x,t,\theta) = x\,\bar{\Phi}(t,\theta) \qquad \Phi_{xr} = \frac{\beta t}{x}\,\bar{\Phi}_{tt}$$

$$\Phi_x = \bar{\Phi} - t\,\bar{\Phi}_t \qquad \Phi_{xx} = \frac{t^2}{x}\,\bar{\Phi}_{tt}$$

$$\Phi_r = \beta\,\bar{\Phi}_t \qquad \Phi_{rr} = \frac{\beta^2}{x}\,\bar{\Phi}_{tt}$$

and

Φ is first order perturbation potention

$\Phi^{(2)} = \Phi + \varphi$ is second order perturbation potential.

And the boundary conditions are

$$\frac{\bar{\varphi}_r}{1 + \varphi_x} = \text{slope of the cone surface}$$

$$\beta\,\bar{\Phi}(\beta\epsilon) = \epsilon\left[\bar{\varphi}(\beta\epsilon) - \beta\epsilon\,\bar{\varphi}_t(\beta\epsilon)\right]$$

$$\bar{\varphi}(\infty) = \bar{\varphi}_t(\infty) = 0 \qquad \text{for second order solution}$$

where the semi-vertex angle of $\tan^{-1}\epsilon$.

By use of an integrating factor $\frac{t}{\sqrt{1-t^2}}$ the homogeneous equation can be integrated to give the result

$$\Phi = -A\left(\text{SECH}^{-1}t - \sqrt{1-t^2}\right)$$

$$A = \frac{\epsilon^2}{\sqrt{1-\beta^2\epsilon} + \epsilon^2\,\text{SECH}^{-1}(\beta\epsilon)} \tag{32}$$

Substituting this result into the above iternation equation, Van Dyke (Ref. 7), gives for the complete second order perturbation potential

$$\bar{\Phi}^{(2)}(t) = -A\left(\text{SECH}^{-1}t - \sqrt{1-t^2}\right)$$

$$+ A^2M_1^2\left[B\left(\text{SECH}^{-1}t - \sqrt{1-t^2}\right) + \left(\text{SECH}^{-1}t\right)^2\right. \tag{33}$$

$$\left. -(N+1)\sqrt{1-t^2}\,\text{SECH}^{-1}t - \frac{\beta^2A}{4}\frac{\sqrt{1-t^2}}{t^2}\right]$$

The streamwise and radial velocity perturbations are

$$\frac{u}{U} = -A\,\text{SECH}^{-1}t + A^2M_1\left[B\,\text{SECH}^{-1}t + \left(\text{SECH}^{-1}t\right)^2\right.$$

$$\left. -(N-1)\frac{\text{SECH}^{-1}t}{\sqrt{1-t^2}} - (N+1) - \frac{3}{4}\beta^2A\frac{\sqrt{1-t^2}}{t^2}\right] \tag{34}$$

$$\frac{1}{\beta}\frac{v}{U} = A\frac{\sqrt{1-t^2}}{t} + A^2M_1\left[-B\frac{\sqrt{1-t^2}}{t} - 2\frac{\sqrt{1-t^2}\,\text{SECH}^{-1}t}{t}\right.$$

$$\left. +(N+1)\frac{1}{t} + (N-1)\frac{t\,\text{SECH}^{-1}t}{\sqrt{1-t^2}} + \frac{1}{2}\beta^2A\frac{\sqrt{1-t^2}}{t^3}\right] \tag{35}$$

The constant B must be adjusted to satisfy the tangency condition given by Eq. (31).

From these expressions the pressure coefficient at any point can be calculated from

$$C_p = \frac{2}{\gamma M_1^2} \left\{ \left[1 + \frac{\gamma-1}{2} M_1^2 \left(1 - \frac{q^2}{U^2} \right) \right]^{\gamma/\gamma-1} - 1 \right\} \qquad (35a)$$

The calculated values of C_p for the cone by the second order theory are given in Table 12. The plot of these values versus Mach number are given on Fig. 16.

G. Hypersonic Similarity

Hypersonic flows are flow fields where the fluid velocity is much larger than the velocity of propagation of small disturbances, the velocity of sound. Tsien, (Ref. 8), has developed the similarity laws for hypersonic flow.

If u, v are the components of velocity in the x, y directions and a is the local velocity of sound, the differential equations for irrotational two-dimensional motion are

$$\left(1 - \frac{U^2}{a^2}\right) u_x - \frac{uv}{a^2} \left(u_y + v_x \right) + \left(1 - \frac{v^2}{a^2} \right) v_y = 0 \qquad (36)$$

$$v_x - u_y = 0 \qquad (37)$$

Introducing the perturbation potential as

$$u = U + \frac{\partial \phi}{\partial x} \qquad v = \frac{\partial \phi}{\partial Y} \tag{38}$$

and the relations

$$a^2 = a_0^2 - \frac{\gamma-1}{2}(u^2+v^2) = a_0^2 - \frac{\gamma-1}{2}\left[u^2 + 2u\phi_x + (\phi_x)^2+(\phi_Y)^2\right] \tag{39}$$

$$a_1^2 = a_0^2 - \frac{\gamma-1}{2} U^2 \tag{40}$$

Since for hypersonic flow both a_1 and $\frac{\partial \phi}{\partial x}$, $\frac{\partial \phi}{\partial Y}$ are small compared to u, the equation of motion becomes to the second order

$$\left[1-(\gamma+1)M_1 \frac{1}{a_1}\phi_x - \frac{\gamma-1}{2}\frac{1}{a_1^2}(\phi_Y)^2 - M_1^2\right]\phi_{xx} -$$

$$2M_1 \frac{1}{a_1}\phi_Y \phi_{xY} + \left[1-(\gamma-1)M_1 \frac{1}{a_1}\phi_x - \frac{\gamma+1}{2}\frac{1}{a_1^2}(\phi_Y)^2\right]\phi_{YY} = 0 \tag{41}$$

Von Kármán, (Ref. 5), has shown that for hypersonic flow over a slender body the variation of fluid velocity due to presence of the body is limited within a narrow region close to the body, the hypersonic boundary layer. Therefore, in order to investigate this velocity variation, the coordinate normal to the body was expanded. If 2b is the length or chord of the body and δ is the thickness of the body, the

non-dimensional coordinates ξ and η can be defined as

$$x = b\xi \qquad Y = b\left(\frac{\delta}{b}\right)^{n}\eta \tag{42}$$

where n is an exponent greater than 0 from above condition of coordinate expansion.

The appropriate non-dimensional form for the velocity potential is

$$\phi = a_1 b \frac{1}{M_1} f(\xi, \eta) \tag{43}$$

By substituting equations 42 and 43 into equation 41, and letting

$$n = 1 \qquad M_1 \frac{\delta}{b} = K$$

Tsien gives the differential equation for two-dimensions as,

$$\left[1-(\gamma-1)\frac{\partial f}{\partial \xi} - \frac{\gamma+1}{2}\frac{1}{K^2}\left(\frac{\partial f}{\partial \eta}\right)^2\right]\frac{\partial^2 f}{\partial \eta^2} = K^2\frac{\partial^2 f}{\partial \xi^2} + 2\frac{\partial f}{\partial \eta}\frac{\partial^2 f}{\partial \xi \partial \eta} \tag{44}$$

with boundary conditions

$$\frac{\partial f}{\partial \xi} = \frac{\partial f}{\partial \eta} = 0 \quad \text{AT} \quad \infty$$

$$\left(\frac{\partial f}{\partial \eta}\right)_{\eta=0} = K^2 h(\xi) \qquad -1 < \xi < 1 \tag{45}$$

where $h(\xi)$ - $1 < \xi < 1$ is a given function describing the thickness distribution along the length of the body.

This similarity law means that if a series of bodies having the same thickness distribution but different thickness ratios (δ/b) are put into flows of different Mach numbers M_1 such that the products of M_1 and (δ/b) remain constant and equal to K, then the flow patterns are similar in the sense that they are governed by the same function $f(\xi, \eta)$ determined by equations (44) and (45).

For axially symmetrical flows, the ordinate y is the radial distance from the axis to the point concerned. Then a similar analysis leads to the following differential equations and boundary conditions.

$$\left[1-(\gamma-1)\frac{\partial f}{\partial \xi} - \frac{\gamma+1}{2}\frac{1}{K^2}\left(\frac{\partial f}{\partial \eta}\right)^2\right]\frac{\partial^2 f}{\partial \eta^2} + \left[1-(\gamma-1)\frac{\partial f}{\partial \xi} - \frac{\gamma-1}{2}\frac{1}{K^2}\left(\frac{\partial f}{\partial \eta}\right)^2\right]\frac{1}{\eta}\frac{\partial f}{\partial \eta} = 2\frac{\partial f}{\partial \eta}\frac{\partial^2 f}{\partial \xi \partial \eta} + K^2\frac{\partial^2 f}{\partial \xi^2} \tag{46}$$

$$\frac{\partial f}{\partial \xi} = \frac{\partial f}{\partial \eta} = 0 \quad \text{AT} \quad \infty$$

$$\left(\eta\frac{\partial f}{\partial \eta}\right)_{\eta=0} = K^2 h(\xi) \qquad -1 < \xi < 1 \tag{47}$$

where $h(\xi)$ is the distribution function for cross-sectional areas along the length of the body.

Shen, (Ref. 9), solves these basic equations by expanding the solution into a series near the initial point and integrating

numerically. The result of this integration determines the flow field, and from this flow field, the surface pressure coefficient can be found. For the cone, Shen gives a curve of C_p/θ^2 vs K, (cf. Fig. 17 and Table 13) which, by using the similarity parameter K, suffices for various slender cones in hypersonic flow. Using this curve the C_p based on hypersonic similitude was readily calculated.

For a wedge Shen's analysis results in the equation

$$C_p/\theta^2 = \frac{\gamma+1}{2} + 2\sqrt{\left(\frac{\gamma+1}{4}\right)^2 + 1/K^2} \qquad (48)$$

where θ = 1/2 apex angle.

The calculations based on the curve and equations are given in Tables 14 to 17, and are plotted on Figs. 18 to 21.

III. CONCLUSIONS

Fig. 22 gives a cross-plot of the surface pressure coefficient for the 20° total apex angle, wedge and cone at zero angle of attack. Examination of this curve indicates:

1. The hypersonic similarity solution gives close agreement with the exact solution for Mach numbers above 6.
2. The second order solution gives close agreement for the low Mach numbers below 4.
3. The linearized theory solution gives, throughout the complete Mach number range, values considerably lower than those of the exact theory.
4. The first and second order theories for the cone give imaginary results for particular values of apex angle and Mach number. In the case of the 20° cone above Mach number of 5.7 for the second order theory and Mach number of 11.0 for the first order theory the solution is imaginary.

Fig. 23 shows the lift coefficient C_L vs M for the 20° wedge at 2° and 4° angles of attack. These curves follow the same pattern in regard to agreement with the exact solution as the calculated values of the pressure coefficients.

REFERENCES

1. Millikan, C. B., "Hydrodynamics of Compressible Fluids", AE 261 Lecture Notes, C.I.T., 1949-1950.

2. Sebert, Harold W., "High Speed Aerodynamics", Prentice-Hall, Inc., pp. 180-197, New York, 1948.

3. Kopal, Z., "Tables of Supersonic Flow Around Cones", Tech. Report No. 1, M.I.T., Department of Electrical Engineering, Center of Analysis, 1947.

4. Liepmann, H. W. and Puckett, A. E., "Aerodynamics of a Compressible Fluid", GALCIT Aeronautical Series, John Wiley and Sons, Inc., pp. 121-124, New York, 1947.

5. Von Kármán, Th., "The Problem of Resistance in Compressible Fluid", Proc. of the 5th Volta Congress, pp. 275-277, Rome, 1936.

6. Busemann, A., "The Achsensymmetusche Kegelge Ukershallstromung", Luftahetforschung, pp. 157-144, 1942.

7. Van Dyke, M. D., "A Study of Second-Order Supersonic Flow", Ph.D. Thesis, California Institute of Technology, 1949.

8. Tsien, H. S., "Similarity Laws of Hypersonic Flows", Jour. of Math. and Phys., Vol. 25, pp. 247-251, 1946.

9. Shen, S. F., "Hypersonic Flow Over a Slender Cone", Jour. of Math. and Phys., Vol. 27, pp. 56-66, 1948.

TABLE 1

Wedge

Oblique Shock Theory

0° Angle of Attack

C_p

	δ						
M	5°	10°	20°	30°	40°	50°	60°
2.0	.0716	.110	.2565	.433	.665		
4.0	.0241	.0558	.1531	.2425	.379	.581	.738
6.0	.0177	.046	.106	.203	.329	.484	.666
8.0	.0148	.0325	.0939	.187	.3095	.463	.641
10.0	.0116	.0294	.0871	.1765	.302	.4515	.634
12.0		.026	.0835	.172	.295	.443	.625

TABLE 2

Wedge

Oblique Shock Theory

2° Angle of Attack

C_p

M		δ 5°	10°	20°	30°	40°	50°	60°
2.0	C_p upper	.0133	.070	.192	.352	.556	.94	
	lower	.104	.168	.320	.51	.800		
4.0	C_p upper	.0045	.038	.100	.194	.324	.476	.652
	lower	.050	.086	.170	.298	.444	.612	.826
6.0	C_p upper	.0028	.026	.078	.162	.276	.420	.590
	lower	.040	.068	.142	.250	.384	.552	.742
8.0	C_p upper	.0022	.018	.066	.146	.260	.396	.566
	lower	.030	.052	.128	.236	.368	.530	.720
10.0	C_p upper	.0015	.012	.060	.140	.256	.390	.560
	lower	.026	.050	.120	.230	.360	.520	.710
12.0	C_p upper	.0011	.012	.060	.140	.256	.390	.560
	lower	.026	.050	.116	.230	.360	.520	.710

TABLE 3

Wedge

Oblique Shock Theory

4° Angle of Attack

C_p

M		δ 5°	10°	20°	30°	40°	50°	60°
2.0	C_p upper		.025	.140	.290	.470	.720	
	lower	.154	.224	.390	.608			
4.0	C_p upper		.0109	.072	.150	.270	.414	.578
	lower	.080	.116	.220	.354	.506	.692	.924
6.0	C_p upper		.0069	.052	.124	.226	.360	.518
	lower	.060	.092	.184	.304	.450	.590	.830
8.0	C_p upper		.0042	.044	.110	.212	.340	.494
	lower	.050	.080	.170	.288	.428	.566	.800
10.0	C_p upper		.0040	.040	.104	.206	.334	.486
	lower	.044	.076	.160	.280	.420	.560	.790
12.0	C_p upper		.0037	.040	.100	.206	.330	.480
	lower	.044	.076	.160	.280	.420	.556	.786

TABLE 4

Cone

Exact Theory (Kopal)

0° Angle of Attack

C_p

M	δ					
	10°	20°	30°	40°	50°	60°
2.0	.0348	.1046	.2026	.3240	.473	.641
4.0	.0250	.0801	.1600	.2670	.382	.551
6.0	.0217	.0720	.1500	.2565	.375	.534
8.0	.0188	.0676	.1465	.2530	.365	.524
10.0	.0186	.0669	.1440	.2520	.363	.519
12.0	.0178	.0658	.1415	.2520	.363	.519

TABLE 5

Wedge

First Order Theory

0° Angle of Attack

C_p

M	δ 5°	10°	20°	30°	40°	50°	60°
2.0	.0503	.1006	.2035	.3090	.4200	.5280	.6650
4.0	.0225	.0449	.0909	.1380	.1880	.2410	.2975
6.0	.0148	.0295	.0596	.0906	.1232	.1580	.1953
8.0	.0110	.0219	.0443	.0673	.0914	.1172	.1450
10.0	.0088	.0175	.0355	.0539	.0732	.0939	.1160
12.0	.0073	.0146	.0295	.0448	.0608	.0780	.0965

TABLE 6

Wedge

First Order Theory

2° Angle of Attack

C_p

M		δ 5°	10°	20°	30°	40°	50°	60°
2.0	C_p upper	0	.0604	.1625	.2665	.3755	.4900	.6130
	C_p lower	.0905	.1420	.2455	.3530	.4670	.5880	.7220
4.0	C_p upper	0	.0269	.0725	.1190	.1678	.2190	.2740
	C_p lower	.0404	.0633	.1096	.1577	.2085	.2625	.3220
6.0	C_p upper	0	.0177	.0476	.0781	.1100	.1435	.1800
	C_p lower	.0265	.0416	.0718	.1035	.1368	.1723	.2115
8.0	C_p upper	0	.0131	.0354	.0580	.0876	.1066	.1335
	C_p lower	.0197	.0309	.0533	.0768	.1015	.1280	.1570
10.0	C_p upper	0	.0105	.0283	.0464	.0654	.0854	.1070
	C_p lower	.0158	.0247	.0426	.0615	.0813	.1025	.1258
12.0	C_p upper	0	.0087	.0235	.0386	.0544	.0709	.0888
	C_p lower	.0131	.0205	.0355	.0511	.0675	.0852	.1045

TABLE 7

Wedge

First Order Theory

4° Angle of Attack

C_p

M		δ = 5°	10°	20°	30°	40°	50°	60°
2.0	C_p upper	-.0302	.0201	.1214	.2240	.3315	.4430	.5630
	C_p lower	.1312	.1830	.2880	.3975	.5140	.6390	.7780
4.0	C_p upper	-.0135	.0090	.0542	.1000	.1480	.1980	.2510
	C_p lower	.0588	.0816	.1288	.1775	.2295	.2855	.3475
6.0	C_p upper	-.0089	.0059	.0356	.0656	.0970	.1300	.1650
	C_p lower	.0385	.0536	.0844	.1165	.1508	.1875	.2280
8.0	C_p upper	-.0066	.0044	.0264	.0488	.0720	.0963	.1225
	C_p lower	.0286	.0398	.0626	.0865	.1118	.1391	.1695
10.0	C_p upper	-.0053	.0035	.0212	.0391	.0577	.0772	.0980
	C_p lower	.0229	.0319	.0502	.0693	.0895	.1115	.1358
12.0	C_p upper	-.0044	.0029	.0176	.0324	.0479	.0642	.0815
	C_p lower	.0190	.0265	.0417	.0575	.0745	.0925	.1127

TABLE 8

Cone

First Order Theory

0° Angle of Attack

C_p

M	δ 5°	10°	20°	30°	40°	50°	60°
2.0	.0134	.0394	.1148	.2036	.2932	.3720	.4400
4.0	.0094	.0268	.0658	.0930	.0952	.0646	
6.0	.0078	.0206	.0402	.0354			
8.0	.0066	.0162	.0220				
10.0	.0038	.0127	.0080				
12.0	.0031	.0099					

TABLE 9

Wedge

Second Order Theory

0° Angle of Attack

C_p

	δ						
M	5°	10°	20°	30°	40°	50°	60°
2.0	.0531	.1065	.2460	.4020	.5810	.7820	1.0000
4.0	.0253	.0519	.1276	.2190	.3300	.4590	.6070
6.0	.0170	.0371	.0960	.1721	.2651	.3775	.5087
8.0	.0133	.0300	.0808	.1481	.2346	.3488	.4625
10.0	.0111	.0257	.0720	.1359	.2168	.3262	.4352
12.0	.0096	.0229	.0660	.1257	.2045	.3108	.4165

TABLE 10

Wedge

Second Order Theory

2° Angle of Attack

C_p

M		δ 5°	10°	20°	30°	40°	50°	60°
2.0	C_p upper	.0101	.0644	.1898	.3371	.5070	.6990	.9160
	lower	.0996	.1627	.3054	.4717	.6600	.8695	1.1040
4.0	C_p upper	.0045	.0304	.0960	.1803	.2832	.4050	.5460
	lower	.0480	.0811	.1615	.2614	.3795	.5161	.6720
6.0	C_p upper	.0030	.0233	.0709	.1389	.2255	.3306	.4554
	lower	.0340	.0593	.1236	.2069	.3085	.4282	.5655
8.0	C_p upper	.0022	.0165	.0586	.1189	.1978	.2954	.4118
	lower	.0271	.0486	.1053	.1809	.2744	.3862	.5162
10.0	C_p upper	.0018	.0138	.0515	.1075	.1820	.2746	.3863
	lower	.0232	.0424	.0946	.1657	.2547	.3622	.4875
12.0	C_p upper	.0015	.0121	.0468	.0994	.1707	.2605	.3693
	lower	.0204	.0383	.0874	.1554	.2411	.3457	.4675

TABLE 11

Wedge

Second Order Theory

4° Angle of Attack

C_p

M			δ 5°	10°	20°	30°	40°	50°	60°
2.0	C_p	upper	-.0292	.0205	.1369	.2752	.4357	.6220	.8265
		lower	.1497	.2113	.3685	.5446	.7400	.9600	1.2010
4.0	C_p	upper	-.0127	.0094	.0674	.1441	.2396	.3555	.4875
		lower	.0742	.1112	.1990	.3070	.4316	.5760	.7388
6.0	C_p	upper	-.0081	.0063	.0487	.1094	.1884	.2872	.4035
		lower	.0539	.0830	.1544	.2458	.3541	.4815	.6266
8.0	C_p	upper	-.0058	.0048	.0395	.0927	.1640	.2551	.3632
		lower	.0441	.0692	.1330	.2163	.3172	.4367	.5740
10.0	C_p	upper	-.0045	.0039	.0342	.0830	.1499	.2358	.3393
		lower	.0383	.0613	.1206	.1995	.2952	.4098	.5422
12.0	C_p	upper	-.0036	.0033	.0307	.0763	.1401	.2222	.3237
		lower	.0344	.0558	.1121	.1878	.2805	.3921	.5217

TABLE 12

Cone

Second Order Theory

$\delta = 10°$		$\delta = 20°$		$\delta = 30°$		$\delta = 40°$	
M	C_p	M	C_p	M	C_p	M	C_p
3.94	.0253	2.14	.1010	1.60	.2270	1.70	.3476
7.68	.0207	3.01	.0881	2.68	.1837	2.80	.3155
11.36	.0209	3.91	.0824	3.83	.1829		
		5.48	.0821				
		5.70	.0829				

TABLE 13

Hypersonic Similarity Parameters

Wedge		Cone (Ref. 8)	
K	C_p/θ^2	K	C_p/θ^2
.1	15.200	.66	2.95
.2	11.280	.92	2.65
.3	7.980	1.22	2.45
.4	6.360	1.59	2.31
.5	5.380	2.10	2.20
.6	4.740	2.74	2.14
.8	3.980	4.00	2.10
1.0	3.536		
1.5	2.992		
2.0	2.762		
3.0	2.581		
4.0	2.500		
5.0	2.464		
6.0	2.446		
7.0	2.432		

TABLE 14

Wedge

Hypersonic Similarity

0° Angle of Attack

5° δ		10° δ		20° δ		30° δ		40° δ		50° δ		60° δ	
M	C_p	M	C_p	M	C_p	M	C_p	M	C_p	M	C_p	M	C_p
2.30	.0289	2.29	.0869	1.70	.249	1.87	.388	2.20	.454	2.14	.775	1.75	1.17
4.59	.0224	3.43	.0615	2.27	.198	2.24	.341	2.75	.402	3.22	.655	2.62	1.00
6.86	.0152	4.57	.0490	2.83	.168	2.99	.287	4.12	.341	4.29	.605	3.49	.916
9.16	.0121	5.71	.0415	3.40	.148	3.74	.254	5.50	.315	6.44	.565	5.23	.857
11.45	.0102	6.86	.0365	4.54	.124	5.60	.215	8.25	.294	8.59	.548	6.99	.830
		9.15	.0306	5.67	.111	7.46	.199	11.00	.285	10.70	.540	8.72	.819
		11.40	.0272	8.50	.0934	11.40	.186					10.45	.812
												12.20	.808

TABLE 15

Wedge

Hypersonic Similarity

2° Angle of Attack

$5^{\circ}\delta$				$10^{\circ}\delta$			
M	C_{p_u}	M	C_{p_L}	M	C_{p_u}	M	C_{p_L}
11.50	.00115	2.50	.0710	1.92	.041	1.63	.170
		3.80	.0530	3.85	.030	2.44	.120
		5.06	.0400	5.76	.022	3.25	.096
		6.32	.0336	7.70	.017	4.06	.081
		7.60	.0282	9.60	.014	4.89	.071
		10.20	.0250	11.50	.013	6.50	.060
		12.60	.0223			8.14	.054
						12.20	.045

TABLE 15 (continued)

Wedge

Hypersonic Similarity

2° Angle of Attack

20°δ				30°δ			
M	C_{p_u}	M	C_{p_L}	M	C_{p_u}	M	C_{p_L}
2.13	.160	1.88	.289	2.16	.285	1.96	.445
2.84	.127	2.35	.245	2.60	.251	2.62	.374
3.55	.108	2.82	.215	3.46	.211	3.28	.332
4.26	.095	3.76	.181	4.34	.187	4.90	.281
5.78	.080	4.70	.161	6.50	.159	6.54	.259
7.10	.071	7.04	.136	8.65	.146	9.80	.242
10.60	.060	9.40	.125	10.80	.137	13.20	.235
		14.00	.117				

TABLE 15 (continued)

Wedge

Hypersonic Similarity

2° Angle of Attack

40°δ				50°δ			
M	C_{p_u}	M	C_{p_L}	M	C_{p_u}	M	C_{p_L}
2.39	.422	1.98	.654	1.88	.720	1.96	.925
3.00	.375	2.47	.580	2.35	.640	2.94	.780
4.58	.317	3.71	.490	3.53	.540	3.92	.721
5.96	.293	4.95	.453	4.70	.500	5.89	.694
8.95	.274	7.42	.424	7.06	.466	7.85	.654
12.00	.265	9.90	.410	9.40	.453	9.80	.646
		12.30	.404	11.75	.445	11.75	.640

60°δ			
M	C_{p_u}	M	C_{p_L}
1.88	1.010	2.40	1.170
2.82	.850	3.20	1.080
3.75	.786	4.80	1.010
5.73	.735	6.40	.980
7.50	.712	8.00	.964
9.40	.700	9.60	.960
11.20	.700	11.20	.952

TABLE 16

Wedge

Hypersonic Similarity

4° Angle of Attack

$5°\delta$				$10°\delta$			
M	C_{p_u}	M	C_{p_L}	M	C_{p_u}	M	C_{p_L}
		2.64	.107	5.70	.0045	1.90	.197
		3.53	.083	11.40	.0035	2.54	.159
		4.40	.070			3.16	.134
		5.26	.062			3.80	.118
		7.03	.052			5.06	.099
		8.80	.046			6.34	.089
		13.10	.039			9.50	.075
						12.60	.069

TABLE 16 (continued)

Wedge

Hypersonic Similarity

4° Angle of Attack

$20°\delta$				$30°\delta$			
M	C_{p_u}	M	C_{p_L}	M	C_{p_u}	M	C_{p_L}
1.90	.123	2.01	.354	2.06	.248	2.32	.475
2.86	.088	2.41	.294	2.58	.210	2.91	.421
3.80	.070	3.21	.247	3.10	.185	4.36	.356
4.76	.059	4.01	.220	4.13	.155	5.80	.329
5.70	.052	6.01	.185	5.16	.138	8.70	.307
7.60	.044	8.02	.171	7.71	.116	11.60	.298
9.50	.039	12.00	.160	10.60	.108		
10.50	.033						

TABLE 16 (continued)

Wedge

Hypersonic Similarity

4° Angle of Attack

40°δ				50°δ			
M	C_{p_u}	M	C_{p_L}	M	C_{p_u}	M	C_{p_L}
2.09	.394	2.25	.705	2.08	.590	2.70	.925
2.79	.330	3.37	.595	2.60	.524	3.61	.854
3.49	.294	4.50	.550	3.90	.443	5.42	.796
5.21	.248	6.74	.514	5.20	.408	7.22	.773
6.96	.229	9.00	.498	7.80	.382	9.01	.760
10.50	.214	11.20	.490	10.40	.370	10.80	.756
				13.00	.364		

60°δ			
M	C_{p_u}	M	C_{p_L}
2.05	.845	2.22	1.37
3.07	.715	2.96	1.26
4.10	.660	4.45	1.18
6.15	.616	5.92	1.14
8.20	.598	7.40	1.12
10.20	.589	8.90	1.11
12.20	.580	10.70	1.11

TABLE 17

Cone

Hypersonic Similarity

0° Angle of Attack

10°δ		20°δ		30°δ		40°δ		50°δ		60°δ	
M	C_p	M	C_p	M	C_p	M	C_p	M	C_p	M	C_p
7.54	.0227	3.74	.0945	2.47	.212	1.81	.336	1.97	.580	2.12	.810
10.50	.0205	5.21	.0849	3.44	.191	2.52	.302	2.61	.536	2.77	.765
13.90	.0188	6.90	.0785	4.55	.176	3.35	.280	3.42	.506	3.66	.729
		9.00	.0740	5.93	.166	4.37	.264	4.50	.482	4.78	.707
		11.88	.0704	7.83	.158	5.77	.251	5.87	.469	6.99	.695
				10.45	.154	7.53	.244	8.58	.460		
						11.00	.239				

TABLE 18

C_L vs M

Wedge, $\delta = 20^\circ$

$\alpha = 2^\circ$

M	Oblique Shock	First Order	Second Order	Hypersonic Similitude
2.0	.1229	.0792	.1102	.0907
4.0	.0673	.0353	.0634	.0730
6.0	.0617	.0229	.0510	.0658
8.0	.0599	.0171	.0443	.0587
10.0	.0580	.0144	.0414	.0556
12.0	.0540	.0114	.0386	.0576

$\alpha = 4^\circ$

M	Oblique Shock	First Order	Second Order	Hypersonic Similitude
2.0	.2391	.1590	.2197	.2221
4.0	.1418	.0714	.1263	.1457
6.0	.1268	.0457	.1006	.1307
8.0	.1211	.0352	.0892	.1300
10.0	.1154	.0276	.0836	.1331
12.0	.1154	.0228	.0778	.1282

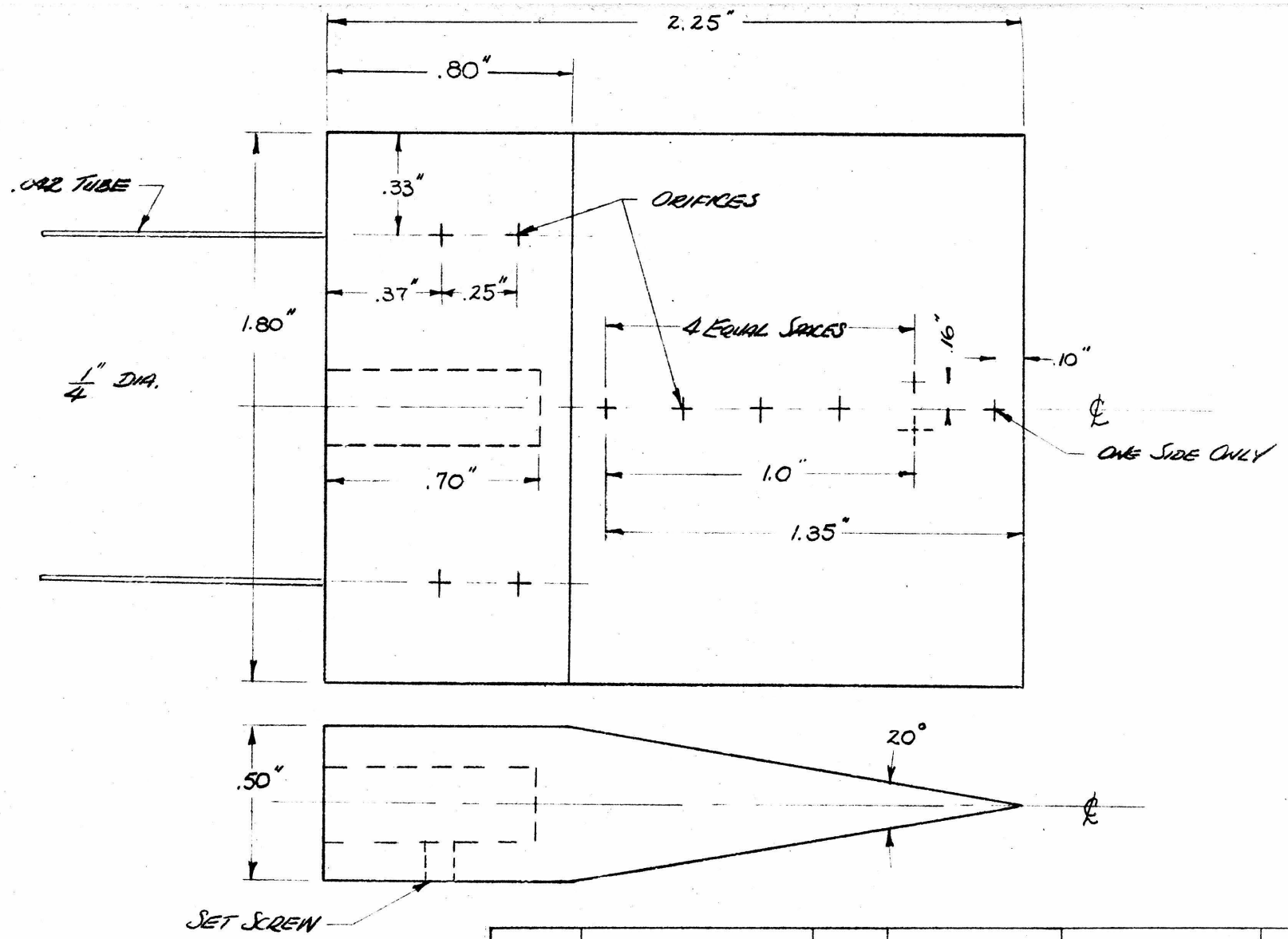

PART NO.	NAME	NO. ROD.	MATERIAL DESC.	MATERIAL SPEC.	WEIGHT

ALL DIMENSIONS IN INCHES
LIMIT ON DIMENSIONS —— { ANGULAR ± ½°, FRACTIONAL ± 1/32, DECIMAL ± .010
UNLESS OTHERWISE NOTED

NUMBERS ARE SURFACE ROUGHNESS IN MICROINCHES

- R — ROUGH MACHINE FINISH
- 250 — SMOOTH MACHINE FINISH
- 40 — ROUGH GRIND
- 16 — FINISH GRIND
- 2 — FINE GRIND, LAP
- 1/4 — POLISH

FINISH

HEAT TREAT

CALIFORNIA INSTITUTE OF TECHNOLOGY

FIG 1 WEDGE
HYPERSONIC MODEL

DRAWN BY
TRACED BY
CHECKED BY
APPROVED BY
DATE
SCALE 2"=1"
COURSE NO.
SECTION NO.
DWG. NO.

D. P. CO.—1000-H

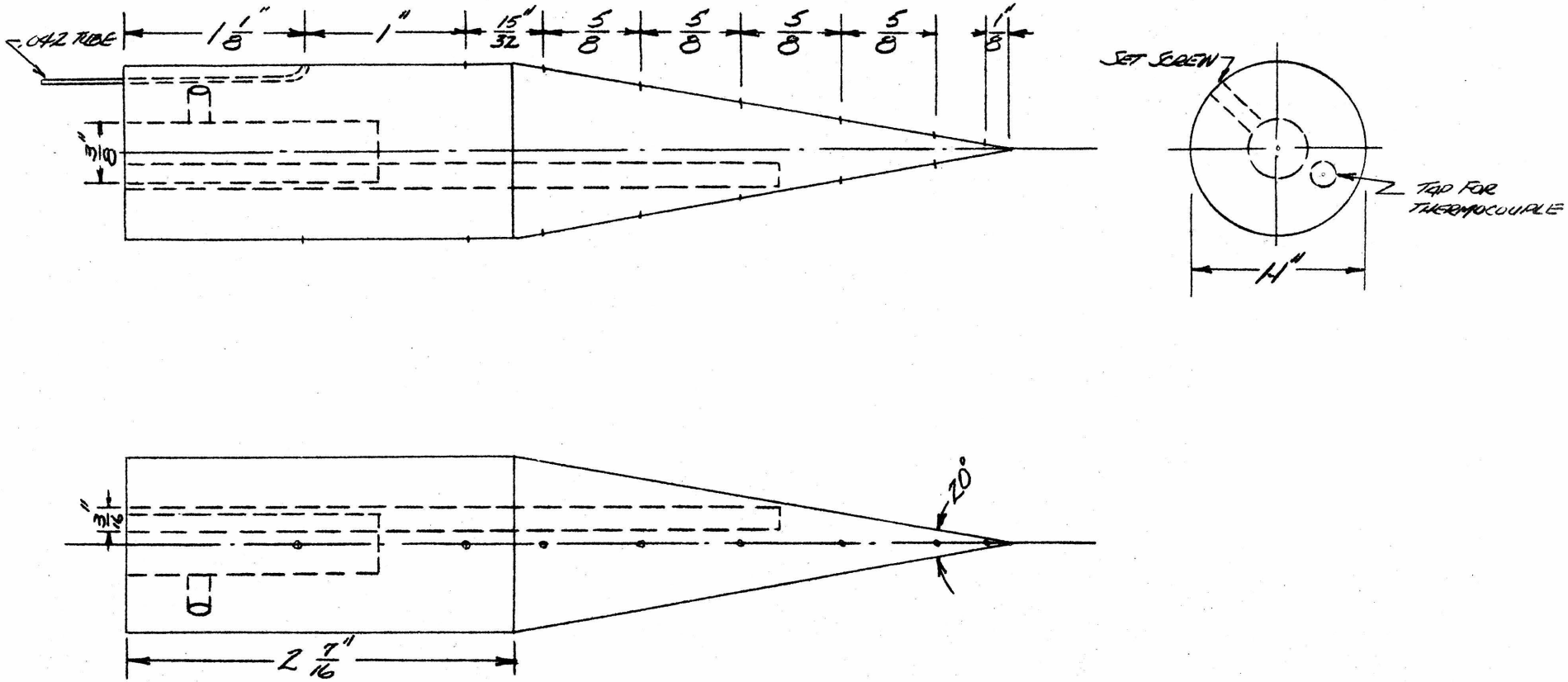

PART NO.	NAME	NO. RQD.	MATERIAL DESC.	MATERIAL SPEC.	WEIGHT

ALL DIMENSIONS IN INCHES	ANGULAR ± ½°
LIMIT ON DIMENSIONS	FRACTIONAL ± 1/32
UNLESS OTHERWISE NOTED	DECIMAL ± .010

NUMBERS ARE SURFACE ROUGHNESS IN MICROINCHES

R ROUGH MACHINE FINISH	16 FINISH GRIND
250 SMOOTH MACHINE FINISH	2 FINE GRIND, LAP
40 ROUGH GRIND	¼ POLISH

FINISH

HEAT TREAT

CALIFORNIA INSTITUTE OF TECHNOLOGY

FIG 2 CONE

HYPERSONIC MODEL

DRAWN BY	
TRACED BY	
CHECKED BY	
APPROVED BY	
DATE	SCALE FULL
COURSE NO.	DWG. NO.
SECTION NO.	

D. P. CO.—1000-H

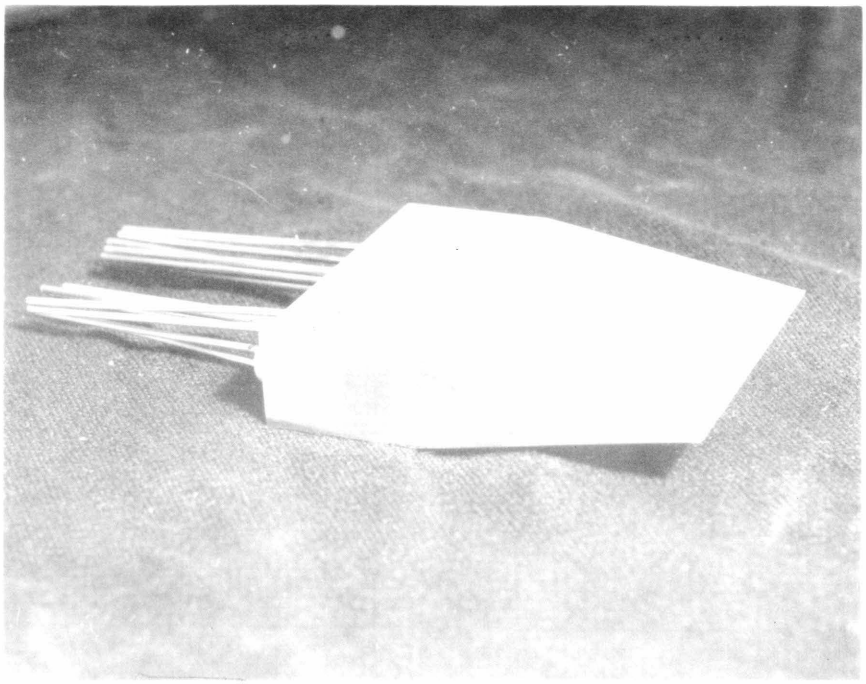

Fig. 3 - 20° WEDGE

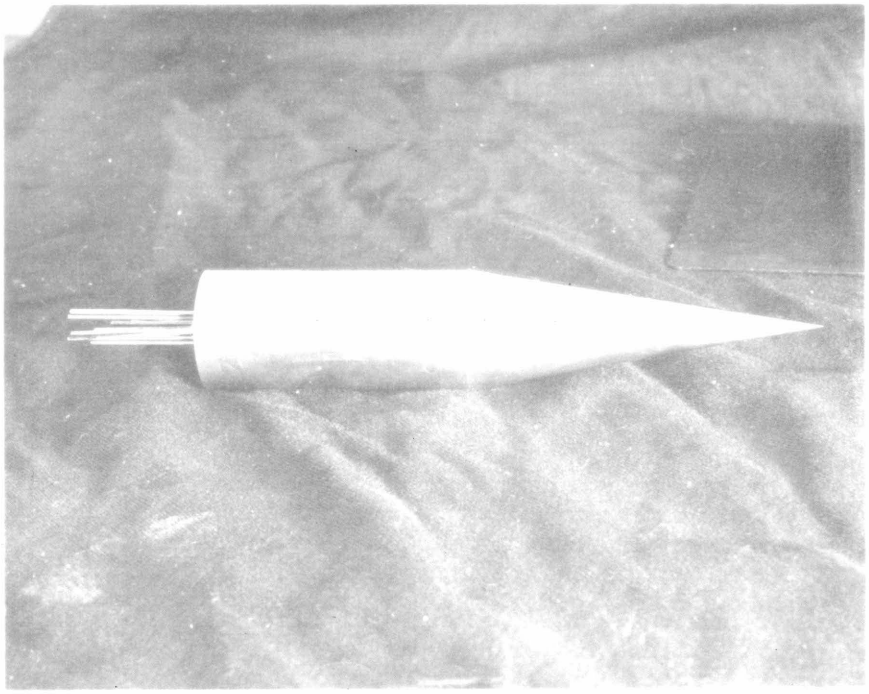

Fig. 4 - 20° CONE

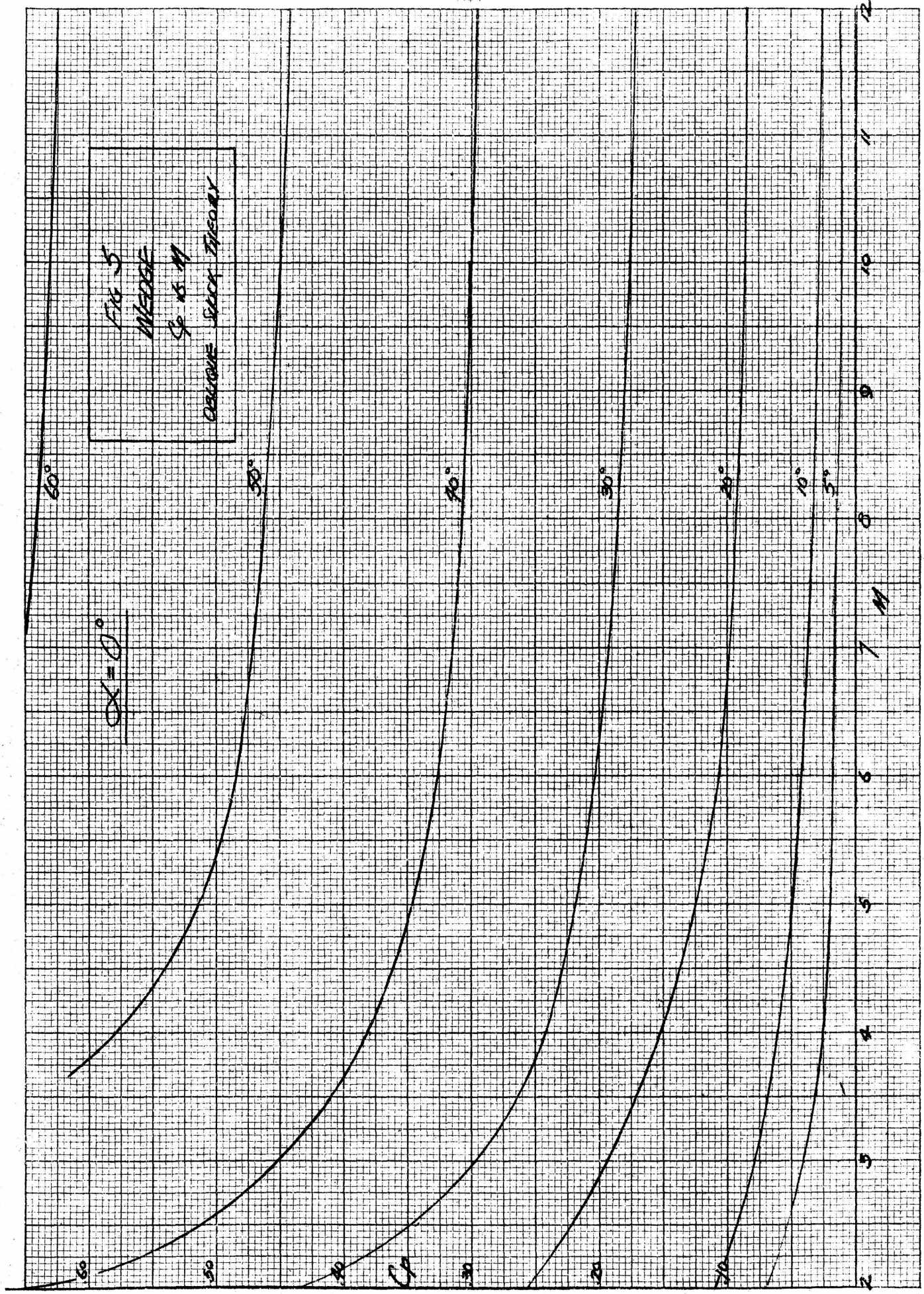
Fig. 5
Mach
Se & M
Oblique Shock Theory
α = 0°
60°
50°
40°
30°
20°
10°
5°
M
12
11
10
9
8
7
6
5
4
3
2
60
50
40
30
20

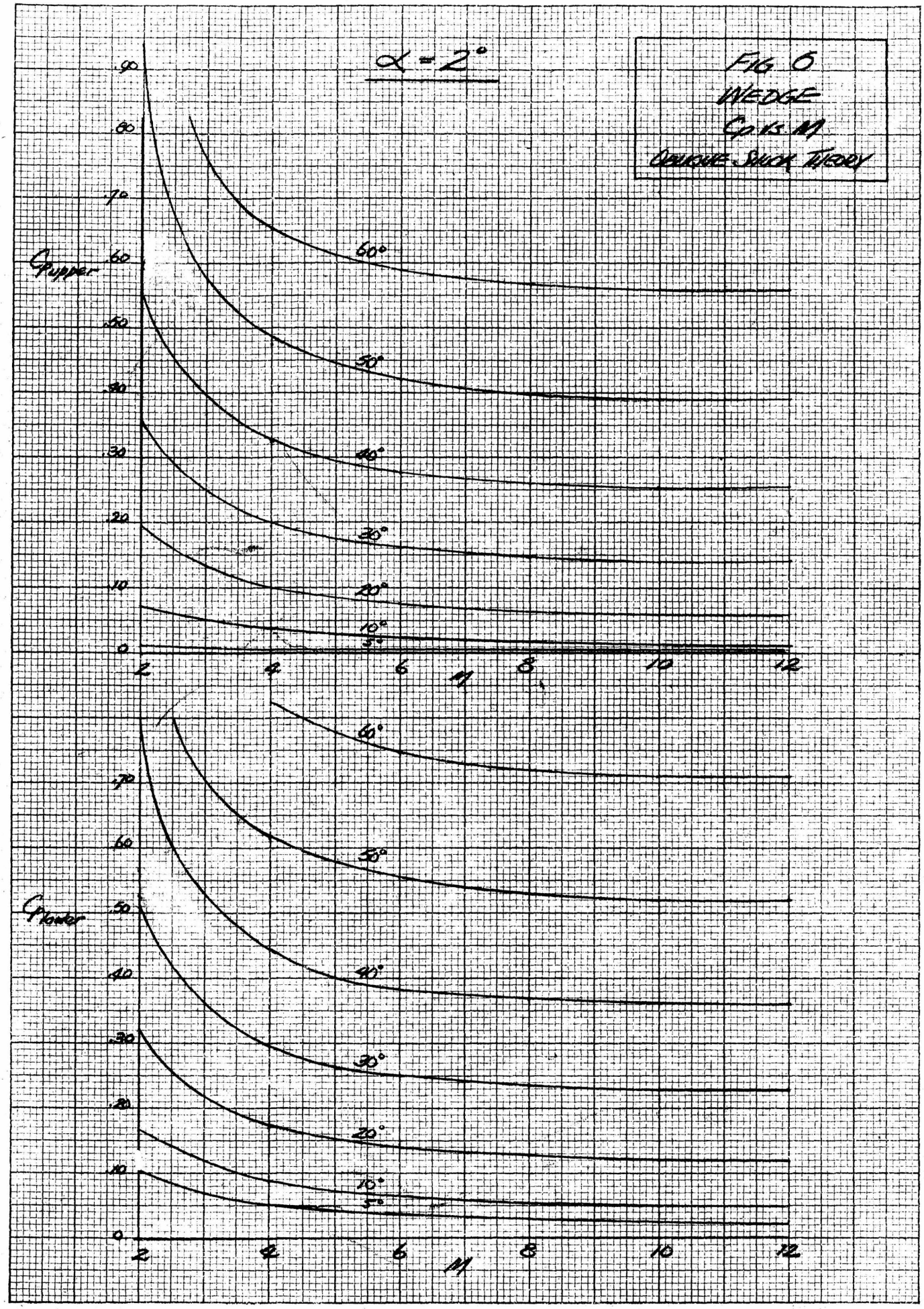
α = 2°
FIG 6
WEDGE
Cp vs M
OBLIQUE SHOCK THEORY
Cp upper
Cp lower
60°
50°
40°
30°
20°
10°
5°
.90
.80
.70
.60
.50
.40
.30
.20
.10
0
2
4
6
M
8
10
12

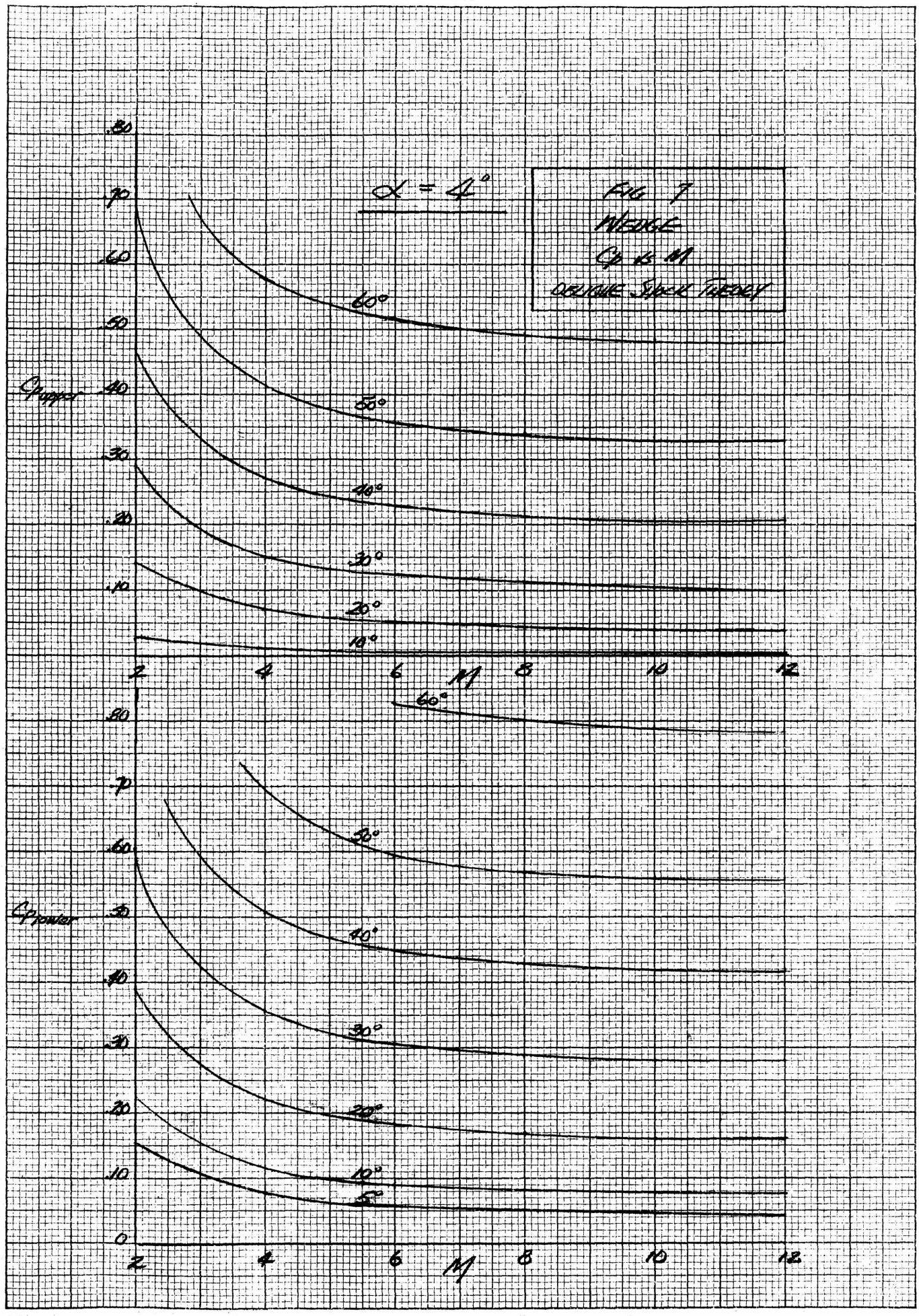
α = 4°
FIG 7
MERGE
Cp vs M
OBLIQUE SHOCK THEORY
Cp upper
Cp lower
60°
50°
40°
30°
20°
10°
5°
2
4
6
M
8
10
12

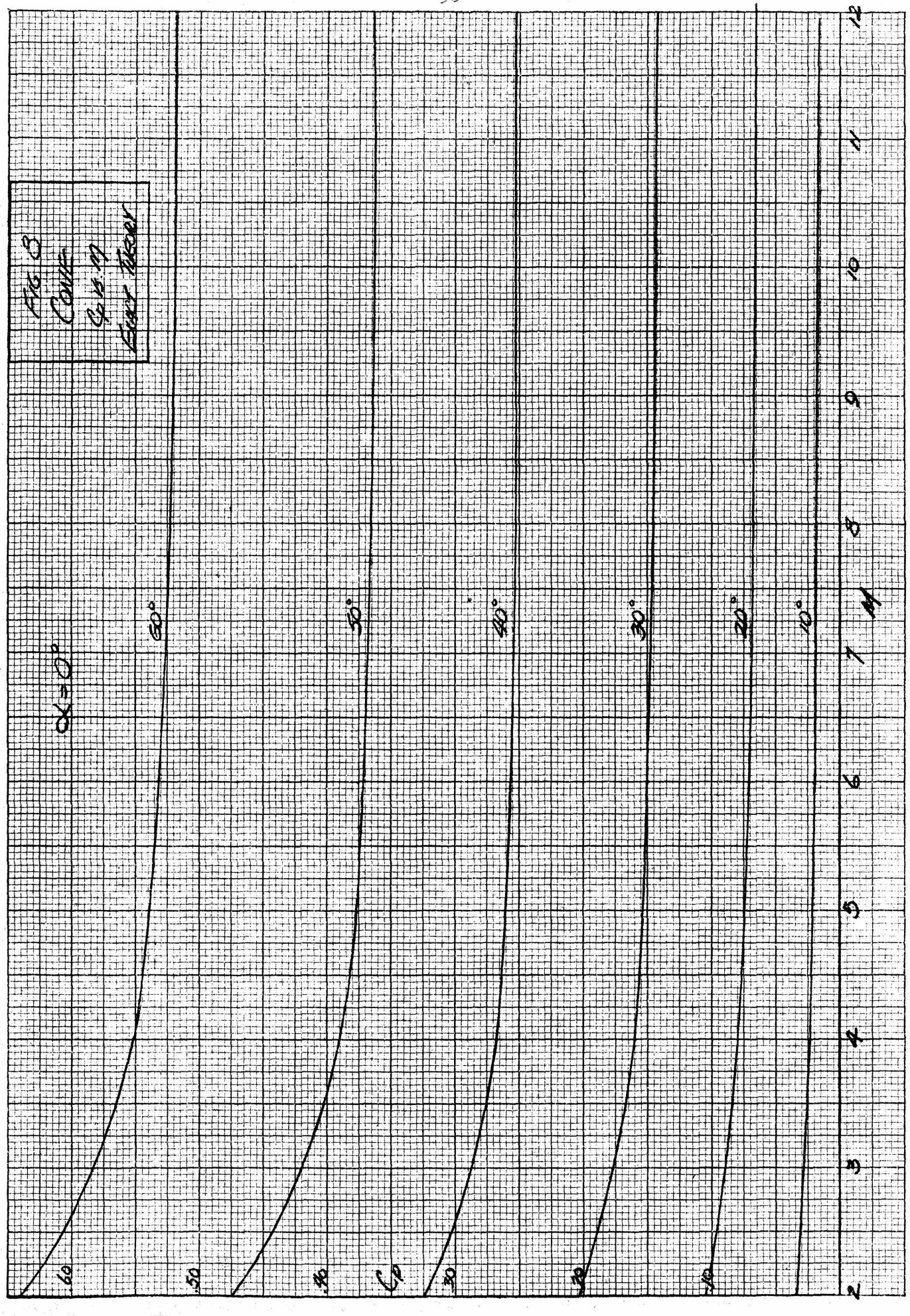
Fig 8
Cone
Cp vs M
Lunt Meyer
α = 0°
60°
50°
40°
30°
20°
10°
Cp
M
.60
.50
.40
.30
.20
.10
2
3
4
5
6
7
8
9
10
11
12

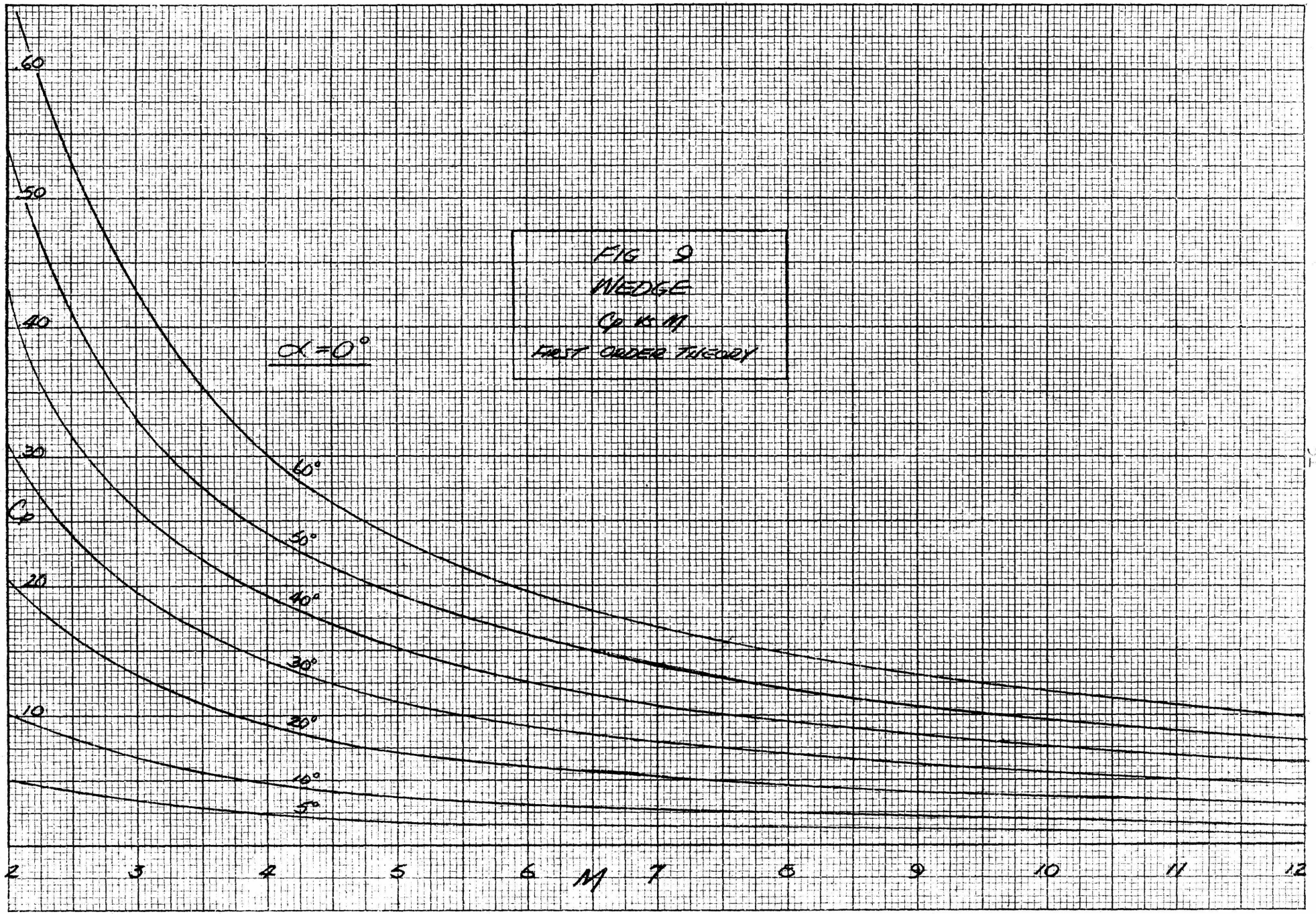
FIG 2
WEDGE
Cp vs M
FIRST ORDER THEORY
α = 0°
Cp
.60
.50
.40
.30
.20
.10
60°
50°
40°
30°
20°
10°
5°
2
3
4
5
6
M
7
8
9
10
11
12

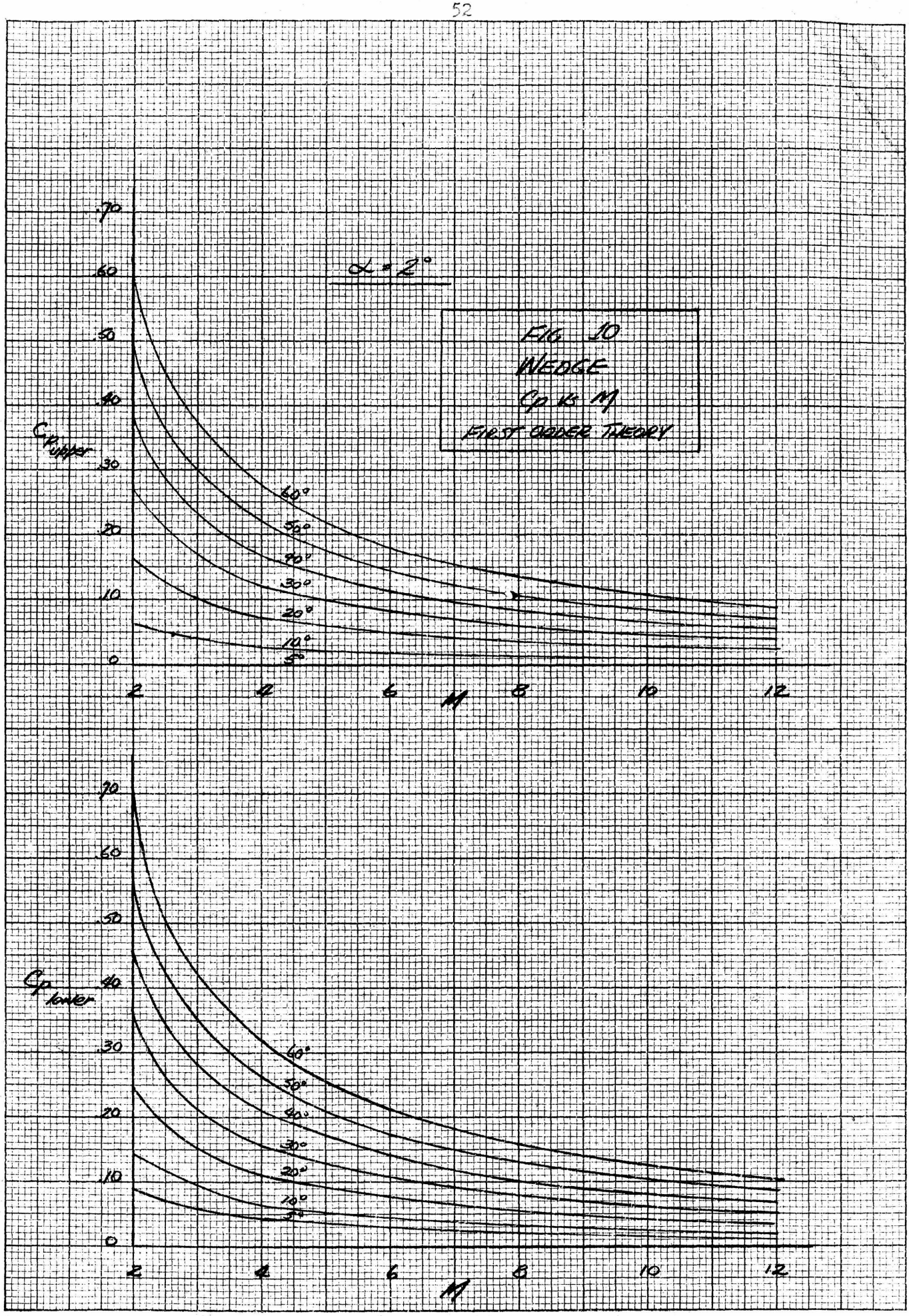
α = 2°
FIG 10
WEDGE
Cp VS M
FIRST ORDER THEORY
Cp upper
.70
.60
.50
.40
.30
.20
.10
0
60°
50°
40°
30°
20°
10°
5°
2
4
6
M
8
10
12
Cp lower
.70
.60
.50
.40
.30
.20
.10
0
60°
50°
40°
30°
20°
10°
5°
2
4
6
M
8
10
12

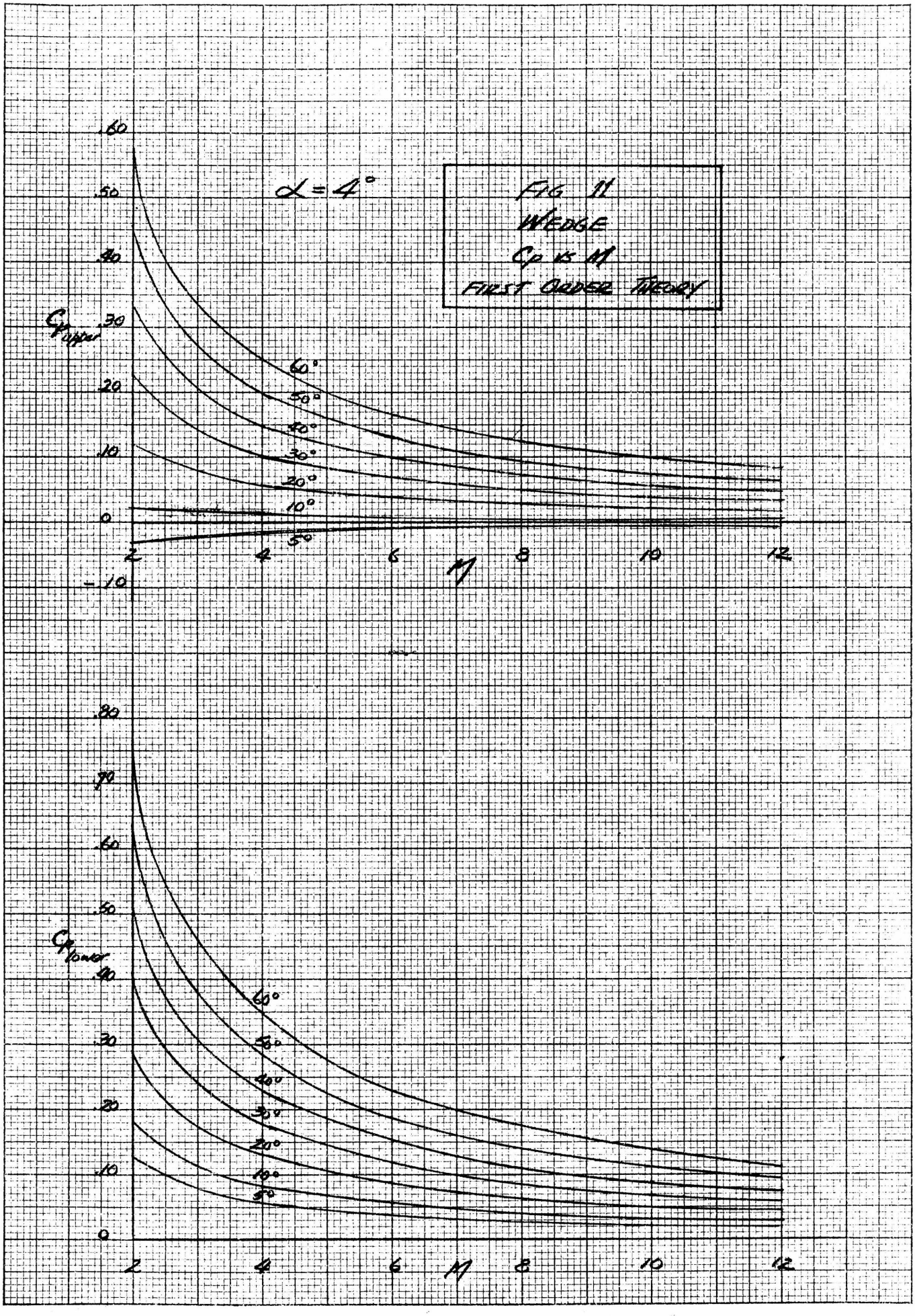
α = 4°
FIG 11
WEDGE
Cp vs M
FIRST ORDER THEORY
Cp upper
Cp lower
60°
50°
40°
30°
20°
10°
0°
M
2
4
6
8
10
12
.60
.50
.40
.30
.20
.10
0
-.10

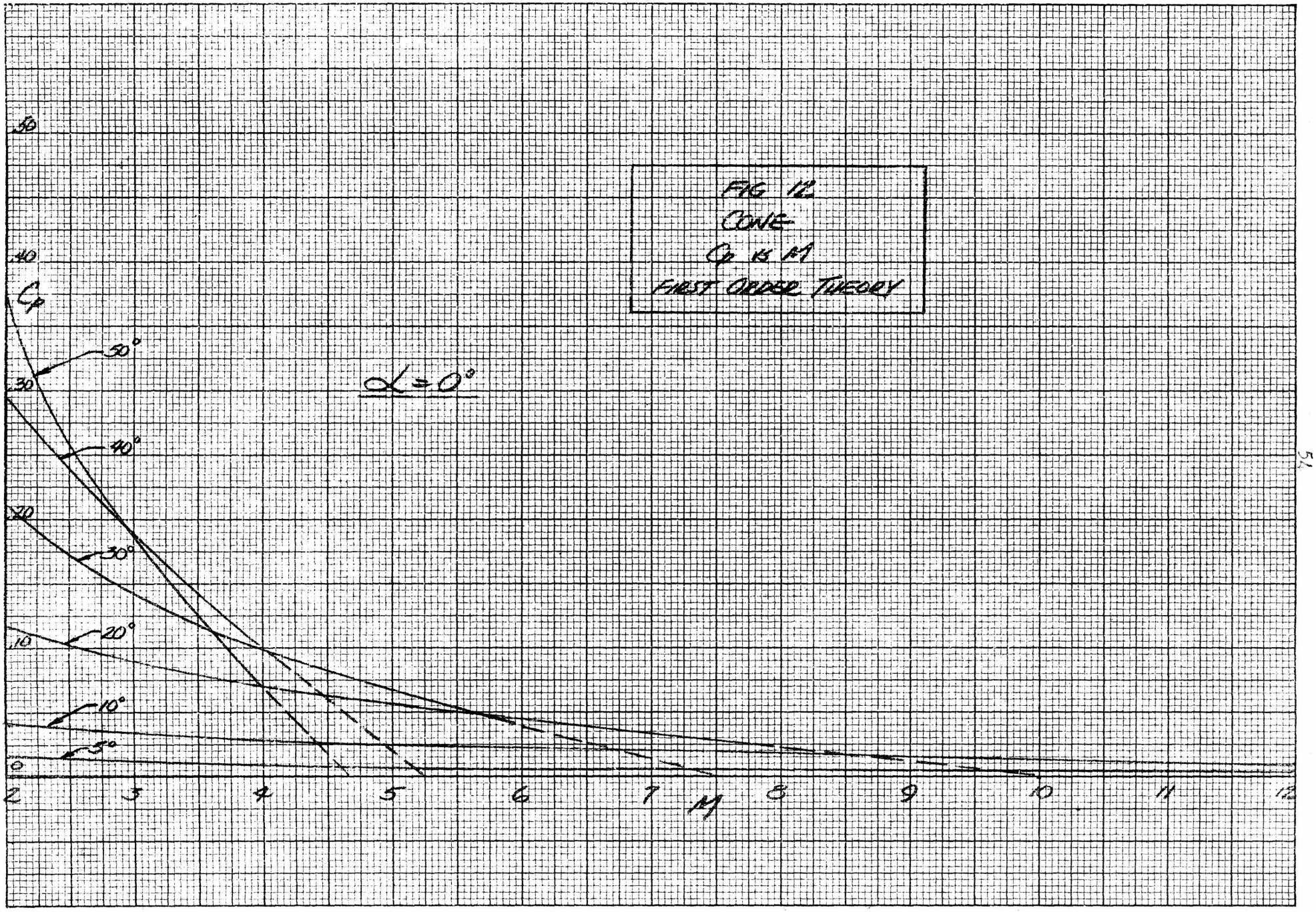
FIG 12
CONE
C_p IS $f(\gamma)$
FIRST ORDER THEORY
C_p
$\alpha = 0°$
50°
40°
30°
20°
10°
5°
50
40
30
20
10
0
2
3
4
5
6
7
M
8
9
10
11
12

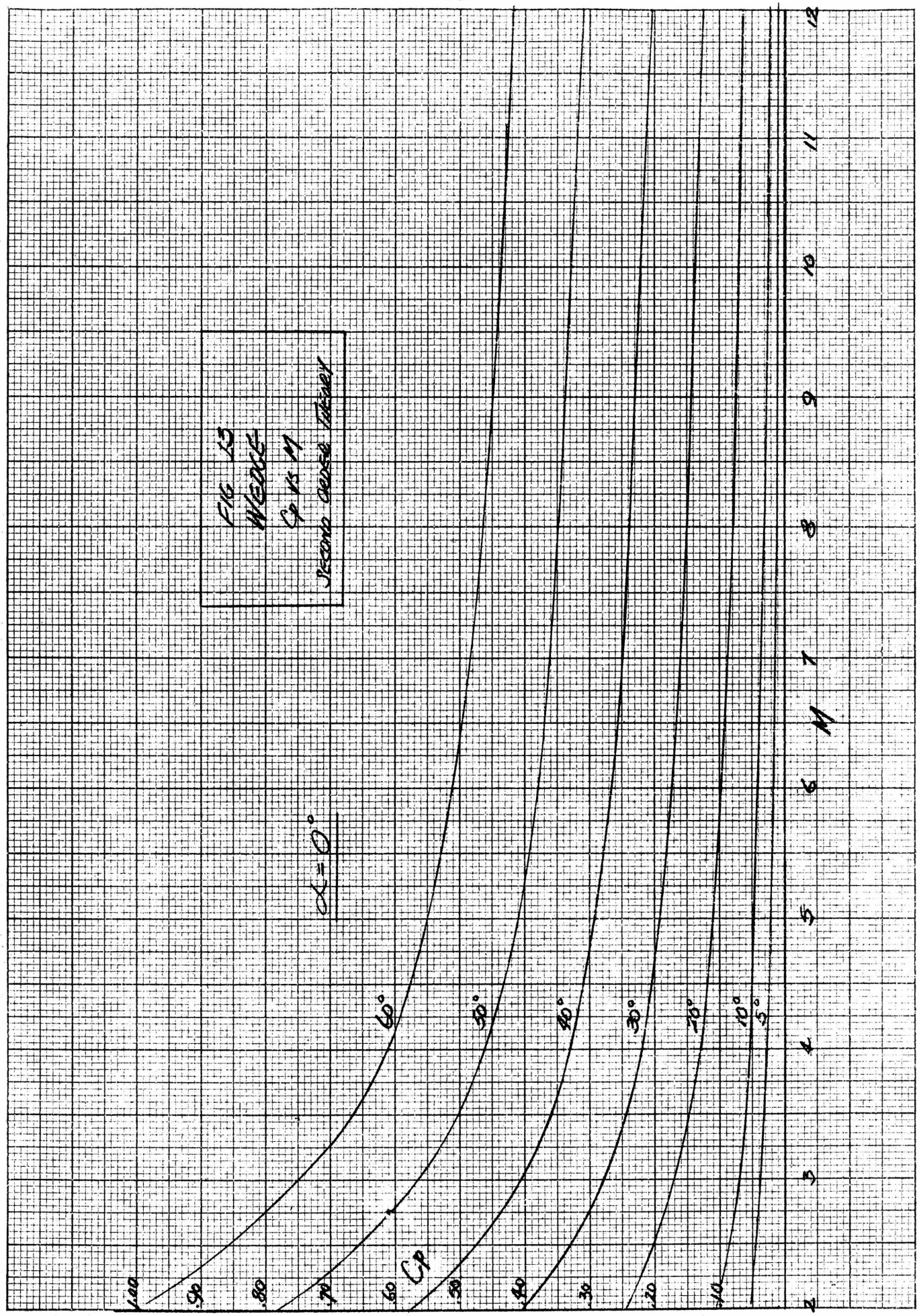
FIG 13
WEDGE
Cp vs M
Second Oblique Shock
α = 0°
60°
50°
40°
30°
20°
10°
5°
Cp
M
100
90
80
70
60
50
40
30
20
10
1
2
3
4
5
6
7
8
9
10
11
12

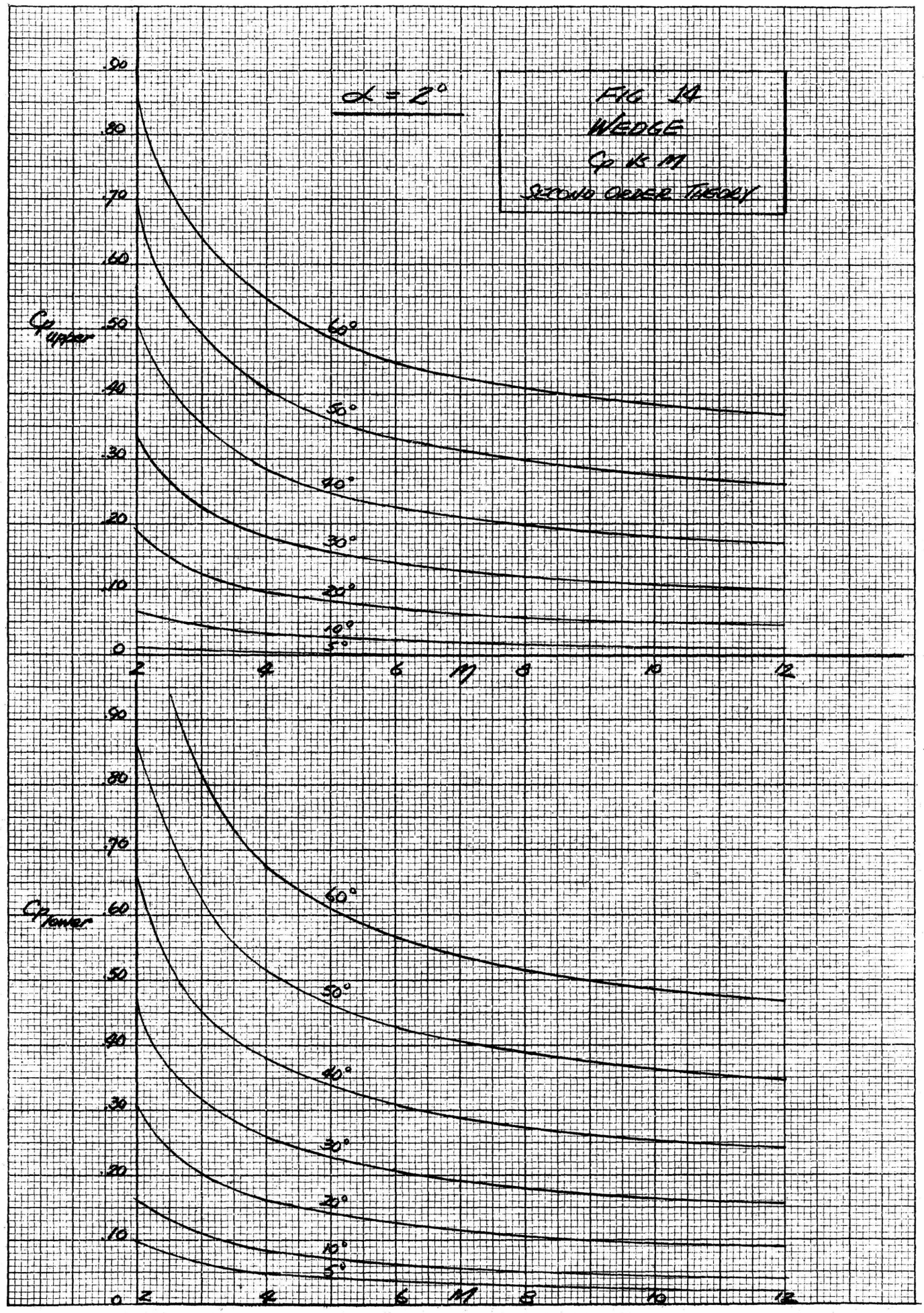
α = 2°
FIG 14
WEDGE
Cp VS M
SECOND ORDER THEORY
Cp upper
Cp lower
60°
50°
40°
30°
20°
10°
5°
.90
.80
.70
.60
.50
.40
.30
.20
.10
0
2
4
6
M
8
10
12

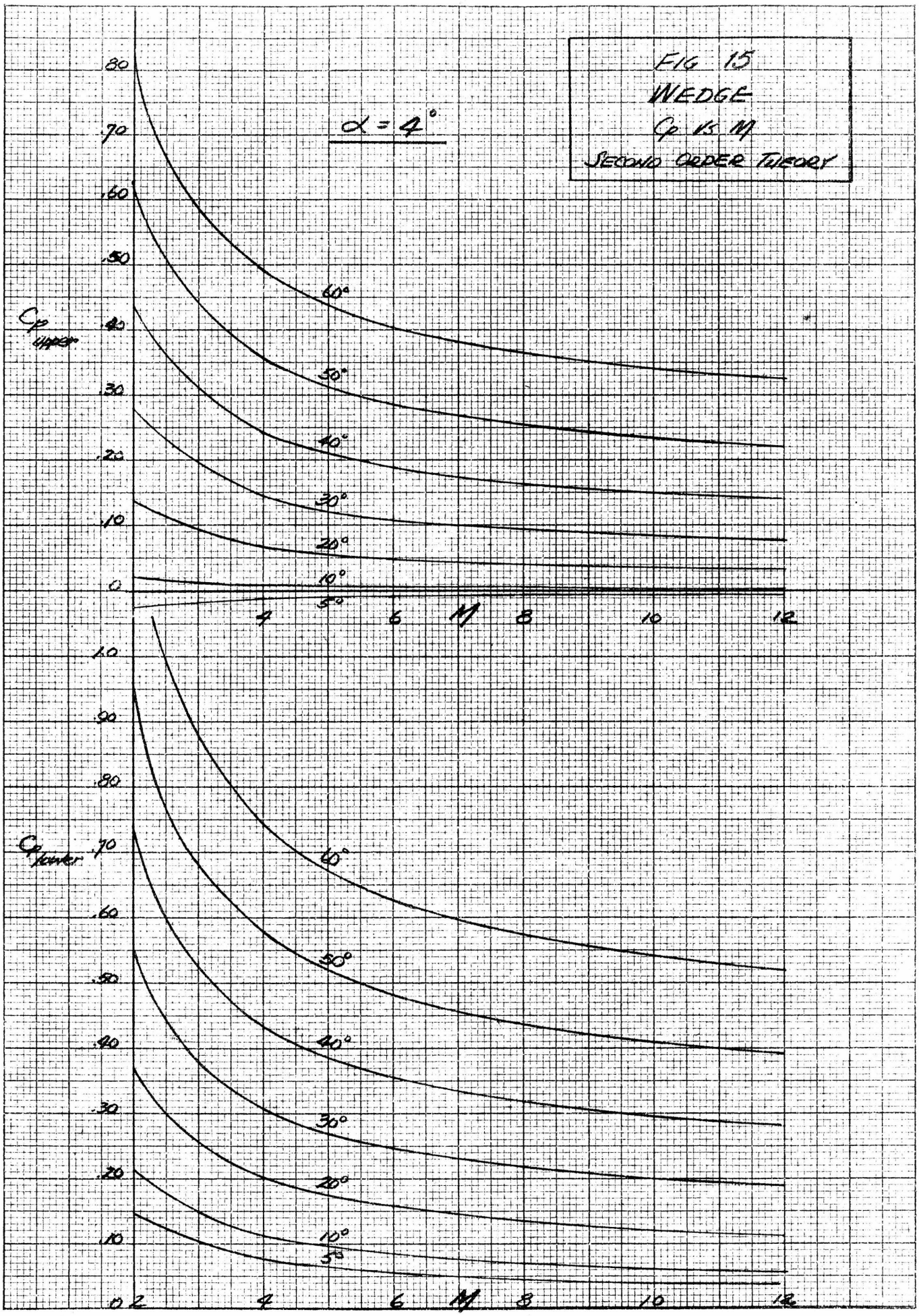
FIG 15
WEDGE
Cp VS M
SECOND ORDER THEORY
α = 4°
Cp upper
Cp lower
80
70
60
50
40
30
20
10
0
60°
50°
40°
30°
20°
10°
5°
4
6
M
8
10
12
2

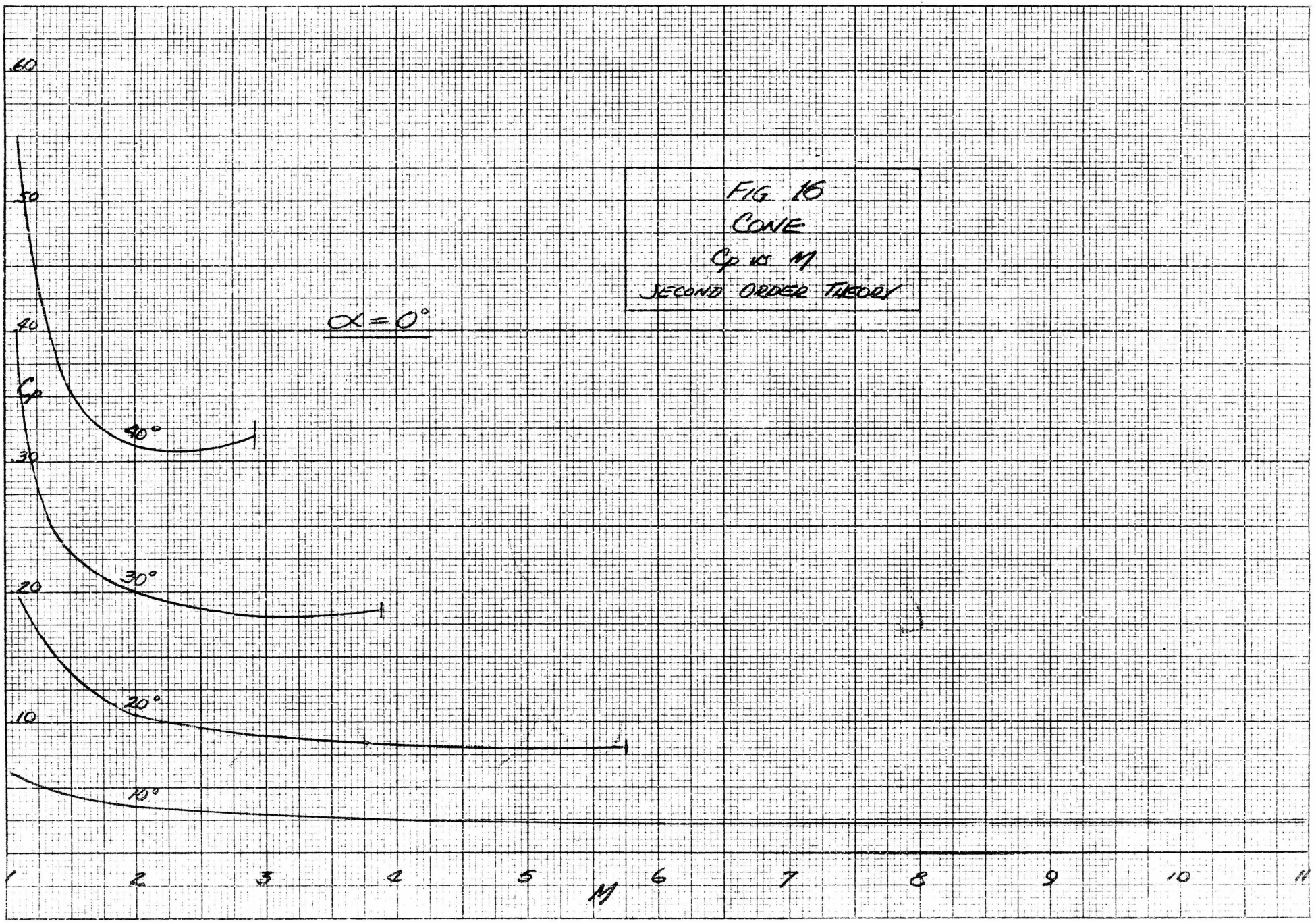
FIG 16
CONE
Cp vs M
SECOND ORDER THEORY
α = 0°
Cp
60
50
40
30
20
10
40°
30°
20°
10°
1
2
3
4
5
M
6
7
8
9
10
11

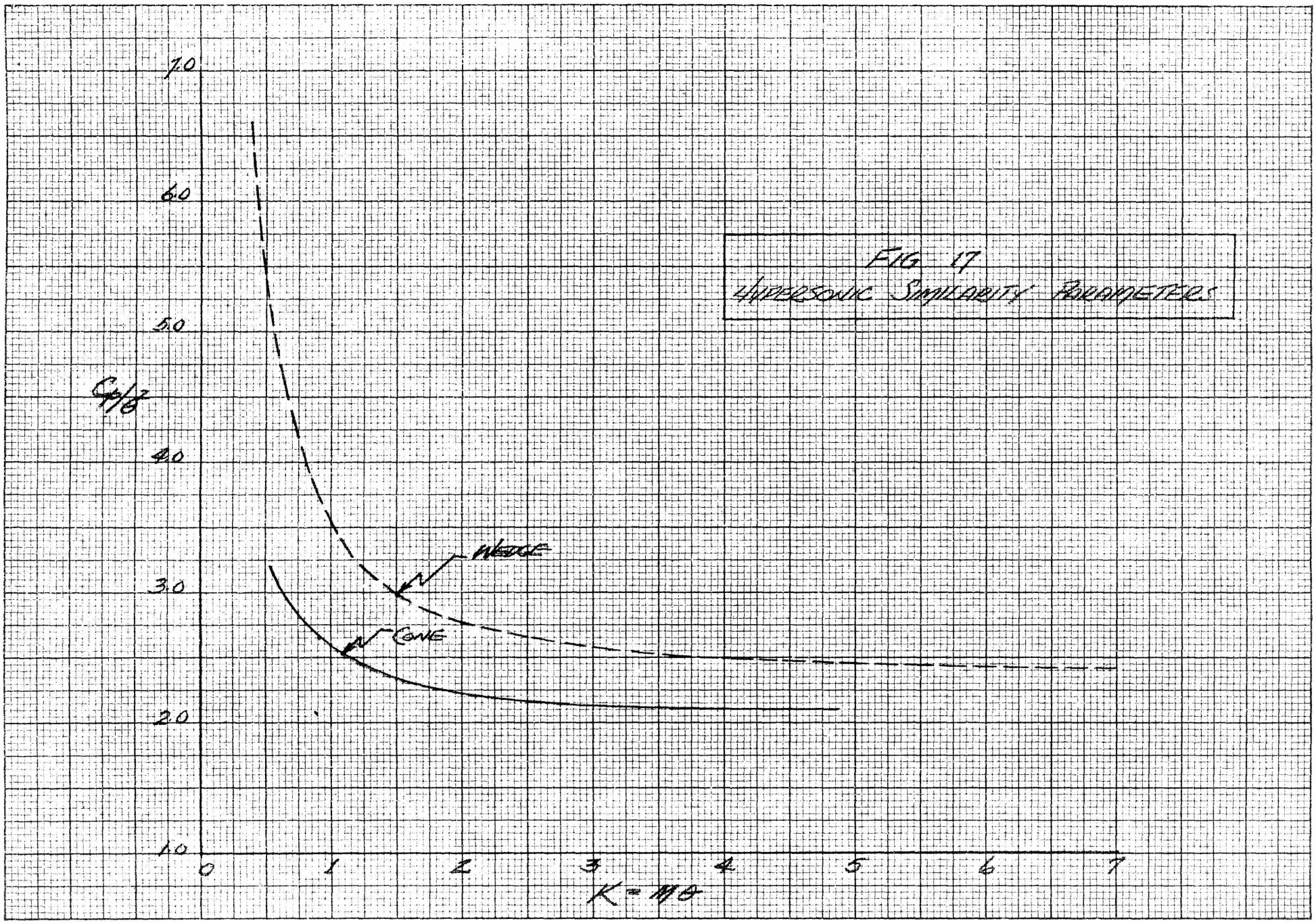

FIG 17
HYPERSONIC SIMILARITY PARAMETERS

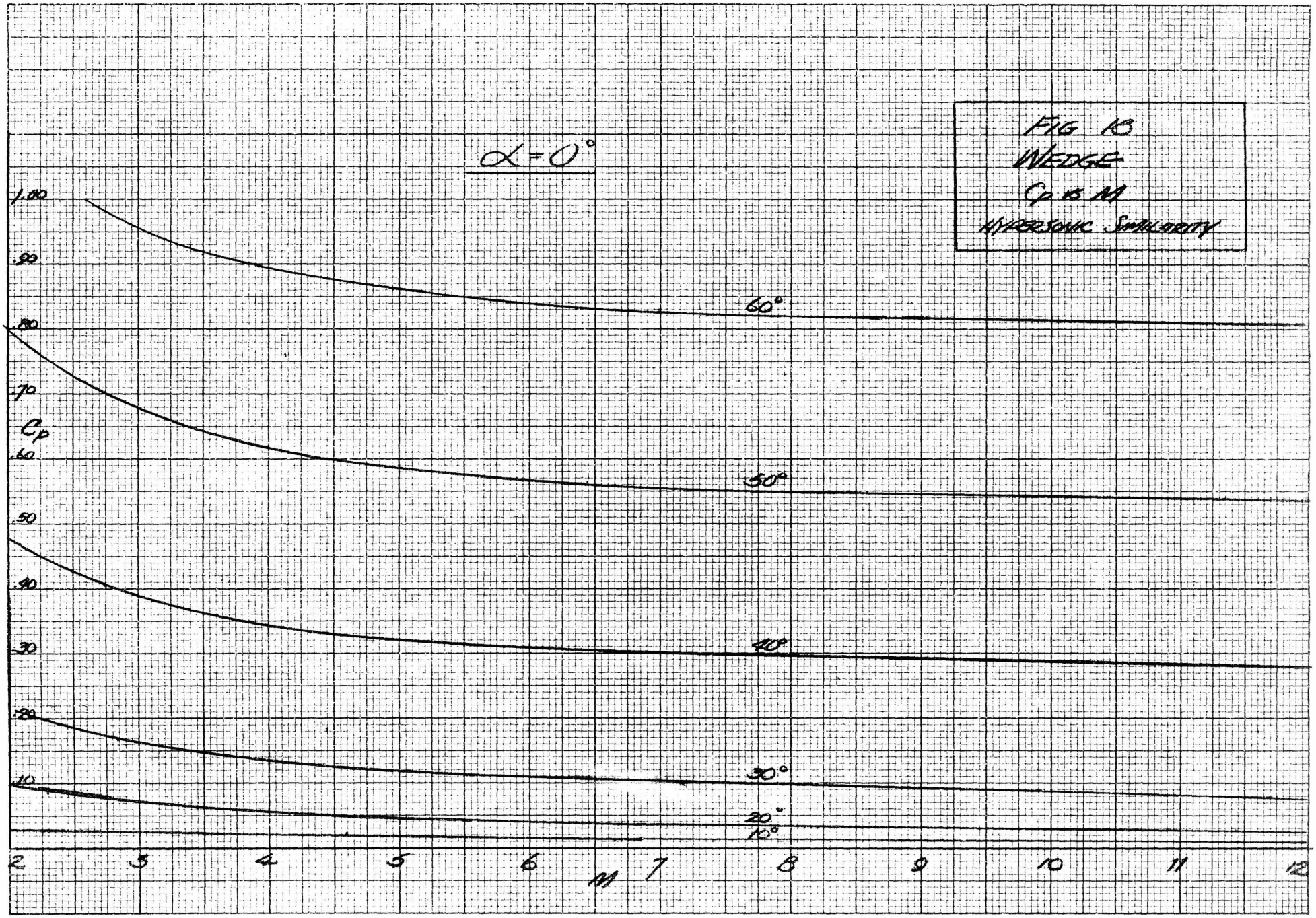
α = 0°
FIG 18
WEDGE
Cp vs M
HYPERSONIC SIMILARITY
1.00
.90
.80
.70
Cp
.60
.50
.40
.30
.20
.10
60°
50°
40°
30°
20°
10°
2
3
4
5
6
M
7
8
9
10
11
12

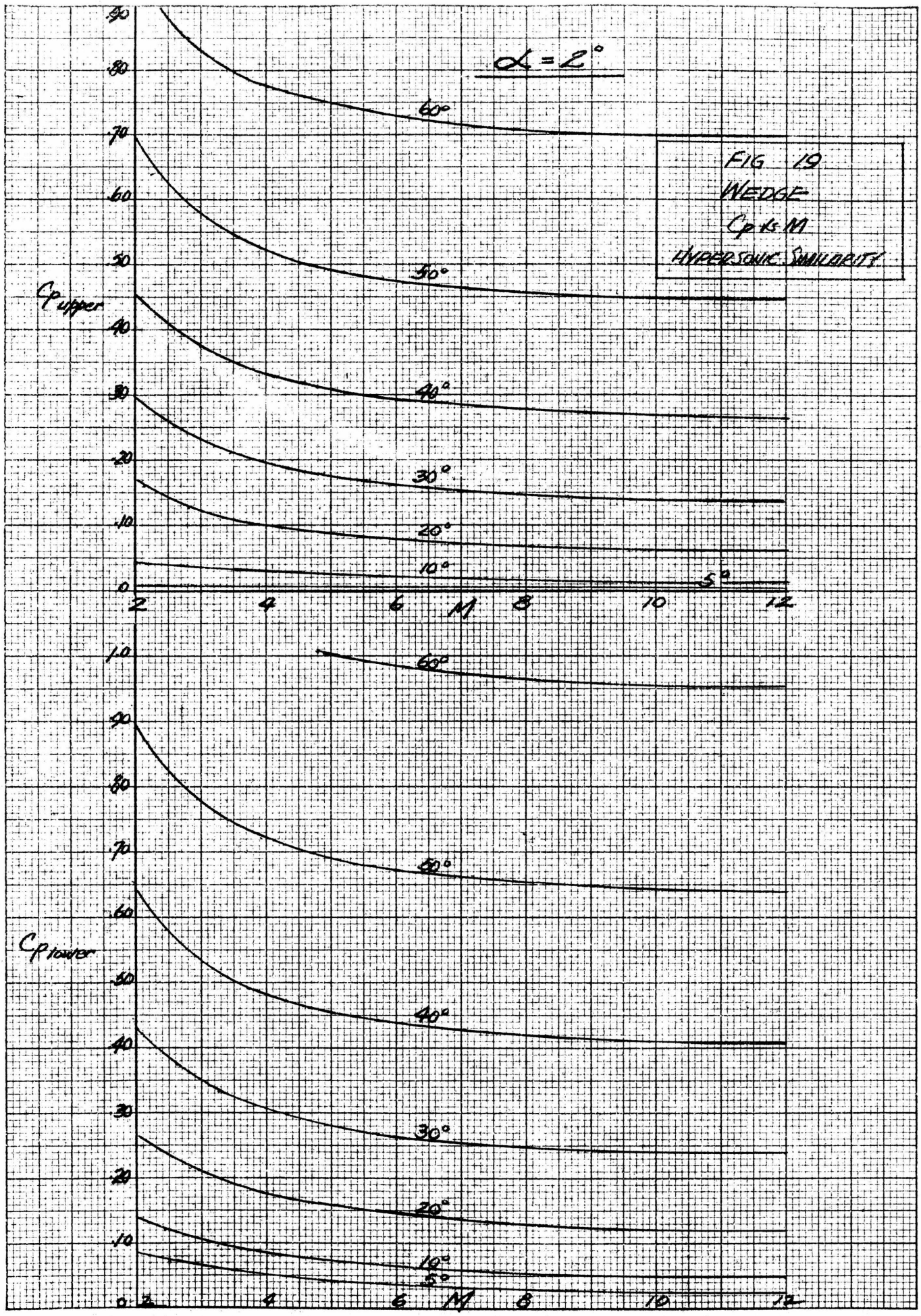
α = 2°
60°
50°
40°
30°
20°
10°
5°
Cp upper
Cp lower
FIG 19
WEDGE
Cp vs M
HYPERSONIC SIMILARITY

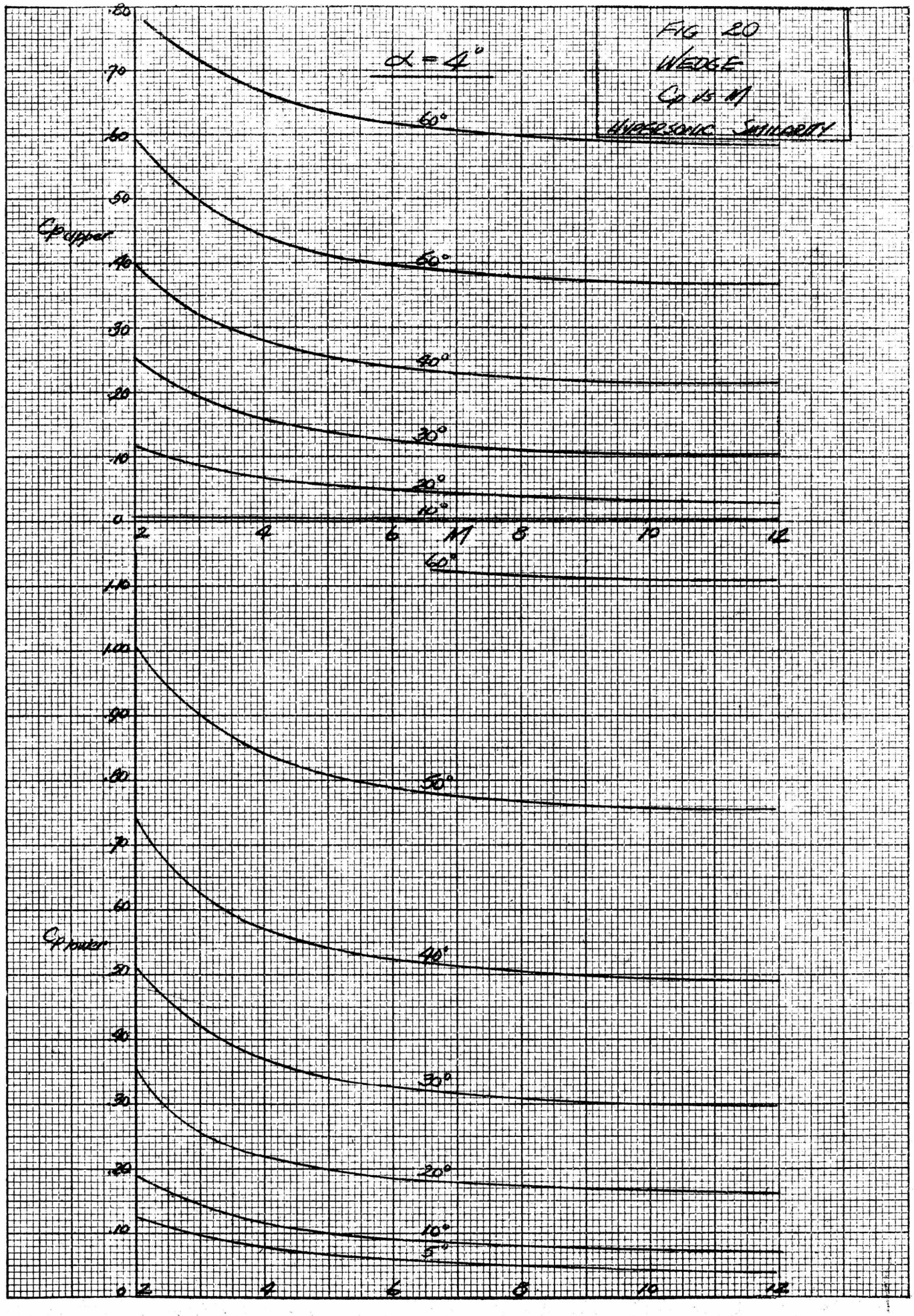
FIG 20
WEDGE
Cp VS M
HYPERSONIC SIMILARITY
α = 4°
Cp upper
Cp lower
80°
70°
60°
50°
40°
30°
20°
10°
5°
0
2
4
6
8
10
12
.80
.70
.60
.50
.40
.30
.20
.10
.100
.90
.80
.70
.60
.50
.40
.30
.20
.10

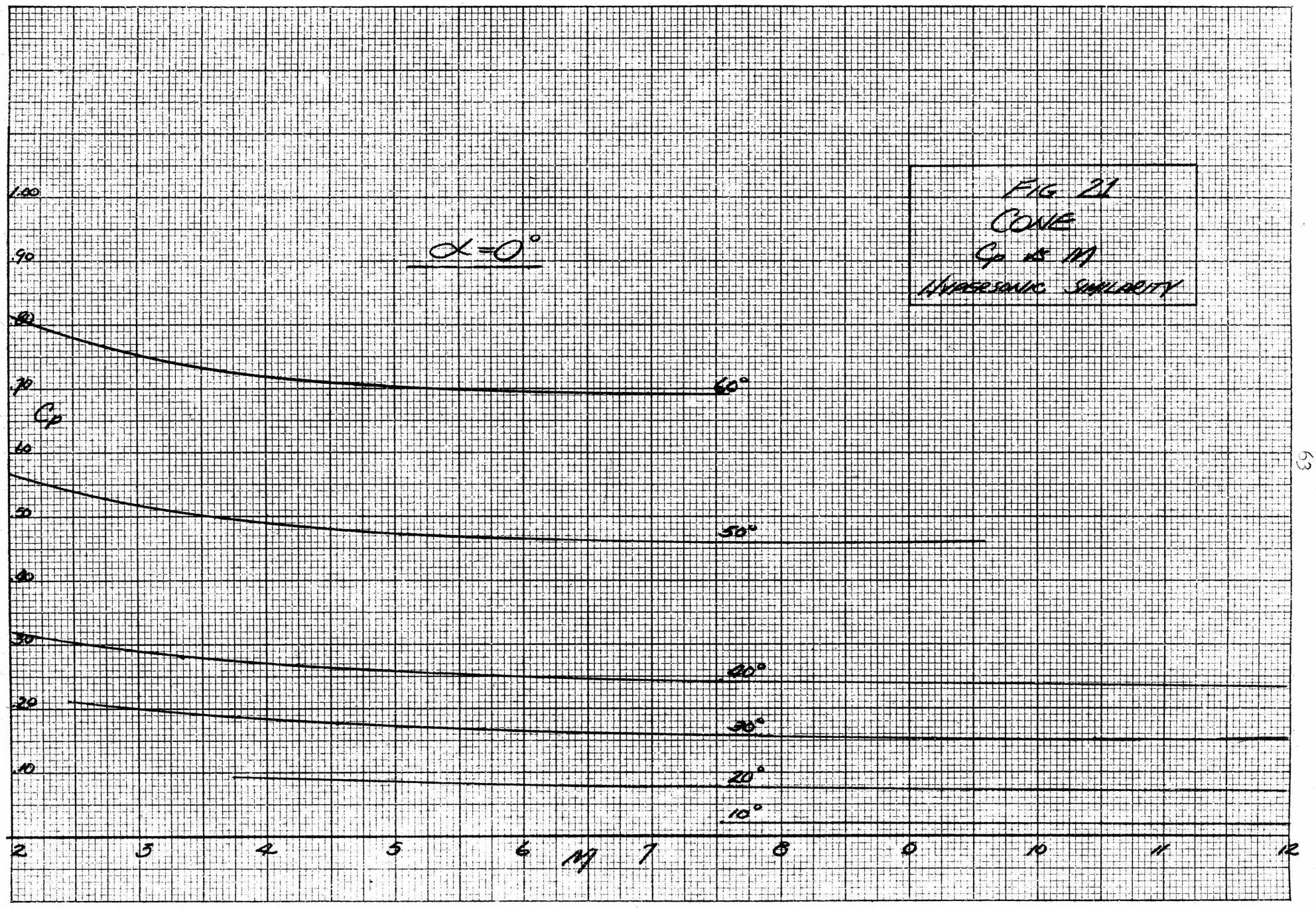
FIG 21
CONE
C_p vs M
HYPERSONIC SIMILARITY
$\alpha = 0°$
60°
50°
40°
30°
20°
10°
C_p
1.00
.90
.80
.70
.60
.50
.40
.30
.20
.10
2
3
4
5
6
M
7
8
9
10
11
12

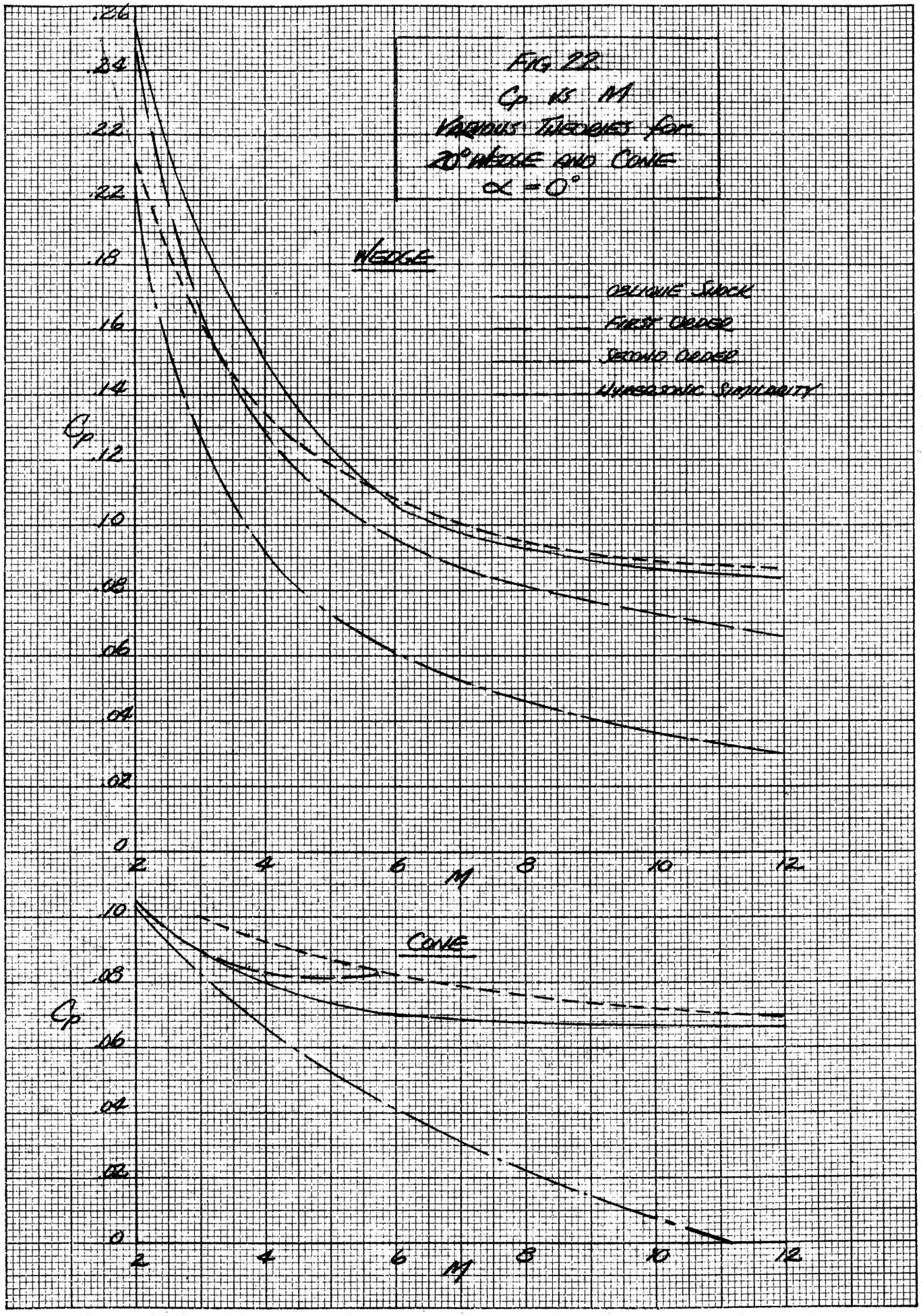
FIG 22
C_p vs M
VARIOUS THEORIES FOR
20° WEDGE AND CONE
$\alpha = 0°$
WEDGE
OBLIQUE SHOCK
FIRST ORDER
SECOND ORDER
HYPERSONIC SIMILARITY
C_p
.26
.24
.22
.20
.18
.16
.14
.12
.10
.08
.06
.04
.02
0
2
4
6
M
8
10
12
CONE
C_p
.10
.08
.06
.04
.02
0
2
4
6
M
8
10
12

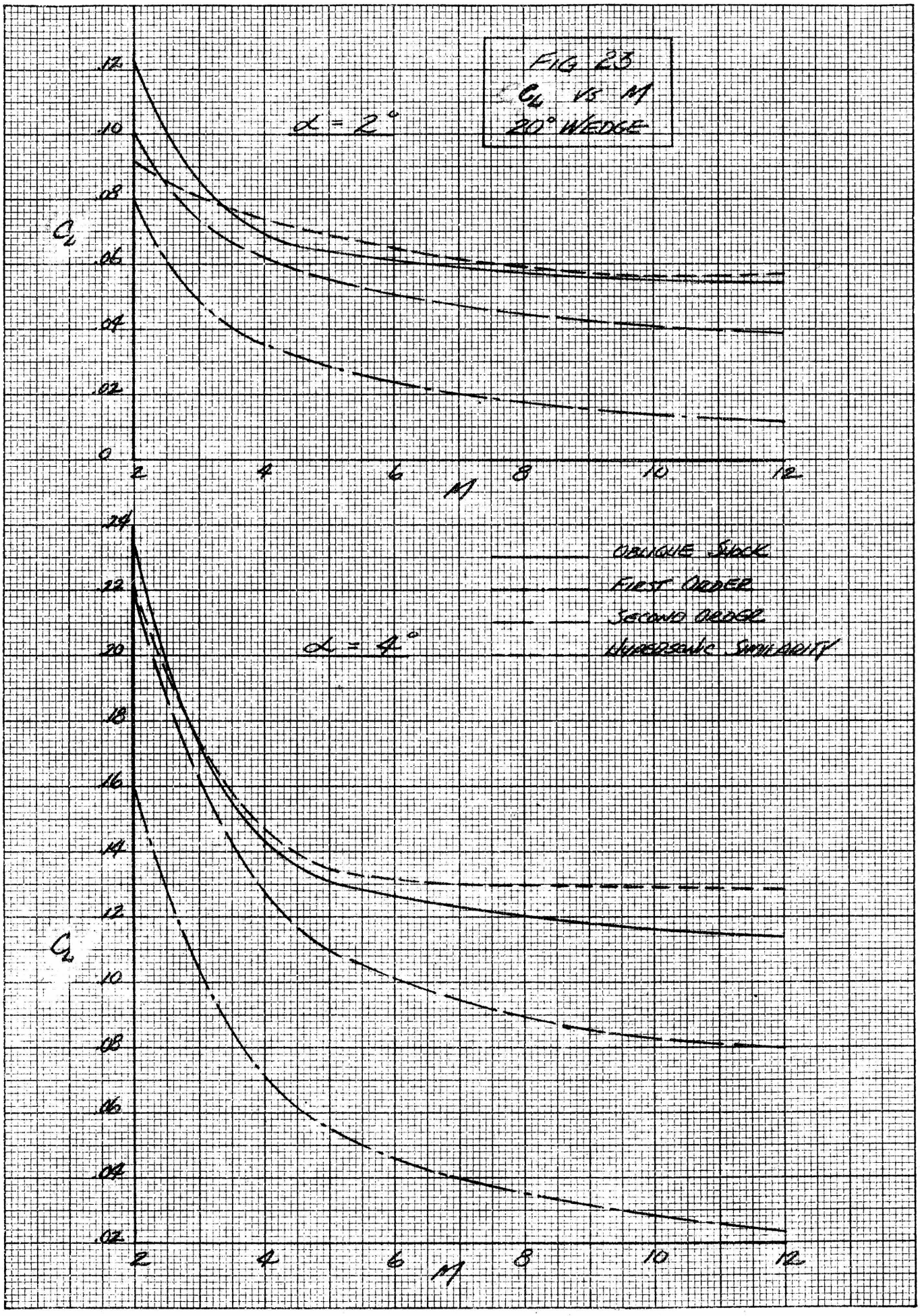
FIG 23
C_L VS M
20° WEDGE
$\alpha = 2°$
$\alpha = 4°$
C_L
M
.12
.10
.08
.06
.04
.02
0
2
4
6
8
10
12
.24
.22
.20
.18
.16
.14
.12
.10
.08
.06
.04
.02
EXACT SHOCK
FIRST ORDER
SECOND ORDER
HYPERSONIC SIMILARITY